### CONFIDENTIAL

Copy RM E54E253



## RESEARCH MEMORANDUM

(NACA-RM-E54E25) COOLING CHARACTERISTICS OF A TRANSPIRATION-COOLED AFTERBURNER WITH A POROUS WALL OF BRAZED AND ROLLED WIRE CLOTH (NASA) 69 p

N73-74689

Unclas 20998

00/99

COOLING CHARACTERISTICS OF A TRANSPIRATION-COOLED

AFTERBURNER WITH A POROUS WALL OF BRAZED

AND ROLLED WIRE CLOTH

By William K. Koffel

Lewis Flight Propulsion Laboratory Cleveland, Ohio

CLASSIFICATION CHANGED

To Undarefied

By authority of Maca Reclassification

#/27 Date 6/5/58

CLASSIFIED DOCUMENT

This material contains information affecting the National Defense of the United States within the meaning of the espionage laws, Title 18, U.S.C., Secs. 793 and 794, the transmission or revelation of which in any manner to an unauthorized person is prohibited by law.

# NATIONAL ADVISORY COMMITTEE FOR AERONAUTICS

WASHINGTON

August 19, 1954

CONFIDENTIAL

.

NACA RM E54E25

CONFIDENTIAL

CLASSIFICATION CHANGED

To <u>Unclassified</u>

By authority of <u>UMCO Relassification</u>

Motice # 127 Date 6/5/58 (a)

NATIONAL ADVISORY COMMITTEE FOR AERONAUTICS

#### RESEARCH MEMORANDUM

COOLING CHARACTERISTICS OF A TRANSPIRATION-COOLED AFTERBURNER WITH A

POROUS WALL OF BRAZED AND ROLLED WIRE CLOTH

By William K. Koffel

#### SUMMARY

Cooling data were obtained for a transpiration-cooled afterburner having a porous combustion-chamber wall of brazed and rolled wire cloth for a range of exhaust-gas temperatures from 1200° to 3340° R, total flow ratio of cooling air to combustion gas of 0.025 to 0.106, and pressure altitudes of 15,000 to 45,000 feet. The data are successfully correlated over a range of Reynolds number from 75,000 to 1,500,000, based on the distance downstream of the leading edge of the porous wall.

Maximum wall temperatures based on the cooling correlation were determined for a porous wall of uniform permeability at sea-level takeoff and for flight Mach numbers of 0.8, 1.5, and 2.0 at an altitude of 35,000 feet. The cooling-air requirements were nearly independent of the flight conditions. A total flow ratio of cooling air to combustion gas of about 0.032 can maintain a maximum wall temperature of 12100 R with an exhaust-gas temperature of 3700° R. The total flow ratios with a uniform permeability distribution and air flows sufficient to limit the maximum wall temperatures to 1210° R are about 15 percent higher than the minimum total flow ratios corresponding to a variable-permeability wall with a constant wall temperature of 1210° R. The total flow ratios for a maximum wall temperature of 1210° R with a wire-cloth afterburner are about 16 percent of the total flow ratios required to cool a stainless-steel afterburner wall convectively to a maximum wall temperature of 1760° R with exhaust-gas temperatures of 3200° and 3700° R. The analysis of cooling-air requirements for the previously mentioned flight conditions indicated that cooling-air static pressures must be closely controlled, especially at a flight Mach number of 2.0.

#### INTRODUCTION

The satisfactory cooling of high-thrust-augmentation afterburners for supersonic aircraft requires large amounts of cooling air. These large quantities of cooling air, whether supplied from the ambient-air

3299

CH-1

stream or from compressor bleed, involve large losses in net thrust. These losses, however, can be minimized through the use of more effective cooling methods. Transpiration cooling has been shown theoretically (ref. 1) to be more effective than film cooling or the conventional method of afterburner cooling by forced convection. The high effectiveness of transpiration cooling was experimentally verified in a preliminary investigation of a transpiration-cooled afterburner having a wall of sintered porous stainless steel (ref. 2). The commercial sintered porous stainless steel used in the preliminary investigation of transpiration cooling for afterburners was unsuitable for use in flight afterburners because of low strength-to-weight ratio, poor control over the uniformity of permeability, and fabrication difficulties.

In the search for more suitable porous materials, wire cloth was investigated (ref. 3) because of its high strength-to-weight ratio, availability in large sheets, ease of fabrication, and low cost compared with sintered porous metals. The NACA Lewis laboratory designed and built a transpiration-cooled afterburner with a porous wall of the brazed and rolled wire cloth, described in reference 3. This burner was operated on a turbojet engine to determine the feasibility of a wire-cloth transpiration-cooled afterburner and to evaluate its cooling performance.

The cooling data from the wire-cloth afterburner are reported herein for pressure altitudes of 15,000 to 45,000 feet, exhaust-gas temperatures from 1200° to 3340° R, and total flow ratios of cooling air to combustion gas of 0.025 to 0.106. A cooling correlation is derived from these data. This correlation is then used to predict the cooling-air requirements of this afterburner with exhaust-gas temperatures of 3200° and 3700° R for several typical flight conditions of a supersonic airplane. A comparison is also made between the cooling-air requirements of this afterburner with transpiration cooling and with conventional forced-convection cooling. The experimental cooling correlation is briefly compared with the approximate theory of Rannie and Friedman (refs. 4 and 5) for transpiration cooling with turbulent boundary-layer flow.

#### APPARATUS AND INSTRUMENTATION

#### Test Installation

The wire-cloth afterburner was mounted on a conventional axial-flow turbojet engine installed in an altitude test chamber. The test installation aft of the turbine flange is shown in figure 1. The engine and afterburner assembly were mounted on a bed plate suspended in the altitude chamber in such a manner as to permit the measurement of jet thrust. A sectional view of the afterburner is shown in figure 2 together with details of the flame holder and fuel-spray bars. The configuration between

the turbine flange and the beginning of the porous wall, including the fuel-spray bars and flame holder, was identical with the high-performance afterburner configuration of reference 6, which was evolved from configuration C of reference 7.

Cooling air from an independent source was filtered through 100 square feet of 1-inch-thick Fiberglas filter media that retained particles greater than 1 micron. The flow was measured by means of an A.S.M.E. standard thin-plate orifice. The plenum chamber and the high-temperature impermeable wall upstream of the porous-wall section were Inconel, and the cooling-air side of the mild steel shroud was painted with zinc chromate primer in order to eliminate the possibility of clogging the wire cloth with fine scale.

The engine fuel was clear unleaded gasoline of 62-octane rating, and the afterburner fuel was MIL-F-5624A, grade JP-4.

#### Wire-Cloth Porous Wall

The porous combustion-chamber wall was made from wire cloth that was brazed and rolled, for permeability reasons, as described in reference 3. The particular cloth used was monel 21x70 twilled Dutch weave (designated cloth B in ref. 3) sprayed with three coats of silver solder per side and brazed and rolled to a 35-percent reduction in original The average final thickness was 0.0274 inch, and the average permeability coefficient K was about 1×10-8 square inch. The tapered combustion chamber was lined with a porous wall made from 20 pieces of wire cloth formed into shallow channels. Each channel was 1/2 inch deep by about 41 inches long and tapered in width from about 4 inches at the upstream end to about 3.5 inches at the downstream end. The channels were spot-welded to angles (fig. 3) that were fastened to the structural shroud by blind rivets. The permeability of each channel differed slightly from the average permeability for all the channels. expected that the cooling-air static pressure would vary somewhat circumferentially because of the tangential inlet to the plenum chamber. Therefore, the channels were arranged in an order that would tend to produce a circumferentially uniform distribution of cooling air.

The newly fabricated porous combustion-chamber wall is shown in figure 4(a). The channels of wire cloth were permanently bulged toward the center line of the combustion chamber after the initial operation of the engine. Figure 4(b) shows the bulged channels at the end of the cooling investigation with cooling passage heights of about 3/4 to 7/8 inch in midchannel. The method of suspending the wire cloth caused a minimum of disturbance to the cooling-air film on the gas side of the porous wall, and the bulging of the channels reduced tensile stresses in the wire cloth caused by pressure forces. The impermeable wall

upstream of the porous wall was forced-convection cooled by the cooling air before it flowed into the 20 dead-ended cooling-air passages.

#### Instrumentation

The research instrumentation for measurement of temperatures and pressures at several stations through the turbojet engine was the same as in reference 6. The location of each temperature and pressure measurement on the afterburner is shown in figure 5. The five principal stations of instrumentation on the porous wall were 24, 32.6, 41, 49.6, and 57.5 inches downstream of the quick-disconnect flange at the combustion-chamber inlet (see fig. 2).

Details of a typical group of instrumentation are shown in figure 6. The cooling-air temperature probes had butt-welded iron-constantan thermocouple junctions shaved smooth to 0.010-inch diameter. thermocouples on the wire cloth were 28-gage (0.013-in.) chromel-alumel wire individually wrapped with silicone-treated asbestos insulation and overbraided with Fiberglas insulation. The orientation and application of the spot-welded junctions on both sides of the wire cloth can be seen in figure 6. There were only four thermocouples on the gas side of the wire cloth because of difficulties in installation. The shroud temperatures were measured with 22-gage (0.025-in.) iron-constantan thermocouples (not shown in fig. 6) spot-welded to the outside of the shroud. The longitudinal profile of static pressure in the combustion chamber was determined by means of 0.080-inch outside diameter by 0.010-inch wall stainless-steel tubes sweat-brazed into the wire cloth and ground flush. The flexibility of these tubes and the method of leading them out of the passage permitted the wire cloth to assume a natural curve with minimum distortion of the cloth at the point of pressure measurement.

Strain-gage pressure pickups were mounted on the cooling-air plenum chamber and on the combustion-chamber wall at the flame-holder station to obtain the static-pressure pulsations in the cooling air and combustion chamber during ignition and normal afterburning. The pressure pulsations were recorded on a two-channel oscillograph.

#### TEST PROCEDURE

Air-flow calibrations were obtained for each piece of wire cloth before fabrication into the porous wall. These calibrations were taken at points where temperature instrumentation was later applied. Additional cold-air-flow calibrations were made of the assembled porous wall, as a whole, at several ambient pressure levels before and during the cooling investigation to detect any over-all change in the air-flow calibrations from plugging by fuel or combustion residues or from oxidation of the

brazing alloy. Nonafterburning check points were also made during the cooling investigation as a check on instrumentation and changes in the wire cloth.

The data are presented in tables I to V, and the approximate range of some of the variables are given in the following table for an inlet cooling-air temperature of  $535^{\circ}$  R:

Pressure altitude, ft	Compressor air flow, lb/sec	air flow, flow, Wa,		Type of test
Sea level	0	0.970-5.810	<sup>a</sup> 535	Check on air-
15,000	0	1.255-4.344	<sup>a</sup> 535	flow calibration
35,000	0	.903-2.849	<sup>a</sup> 535	and plugging of
45,000	0	1.49-1,79	<sup>a</sup> 535	wire cloth
15,000	45.8	1.2-3.8	1200	Cooling, non-
35,000	25.5	.83-2.7	1250	afterburning
15,000 35,000 45,000	45.8 25.5 15.6	1.37-3.25 1.26-3.16 1.49-1.79	2580-3010 1800-3340 3185	Cooling, afterburning

<sup>&</sup>lt;sup>a</sup>Approximate ambient-air temperature.

The cooling-air flow was varied at a given pressure altitude and fuel-air ratio between the following limits:

- (1) Minimum static-pressure difference △p across upstream edge of wire cloth of 0.5 lb/sq in. to prevent reverse flow of combustion gas through wire cloth
- (2) Maximum  $\Delta p$  across downstream edge of wire cloth of 6 lb/sq in. to avoid bursting channels of wire cloth
- (3) Maximum wire-cloth temperature of 1460°R to avoid excessive rate of plugging from oxidation of silver solder
- (4) Maximum turbine-outlet gas temperature of 1625° R to protect turbine from over-temperature

#### METHODS OF CALCULATION AND ANALYSIS

#### Cooling-Air Flow

Local values of the cooling-air flow normal to a unit of wire-cloth surface area  $(\rho V)_a$  were computed for two channels, channel 1 having the hottest and channel 9 having the coldest porous-wall temperatures. This computation was based on the air-flow calibrations of figure 7, the thickness of each channel, the respective longitudinal profiles of cooling-air static pressure, and the assumption that the longitudinal profile of combustion-gas static pressure was circumferentially uniform.

The ordinate  $\frac{\Delta(p^2)}{\tau} \left(\frac{\mu_o}{\mu}\right)^2 \frac{T_o}{T}$  of (Symbols are defined in appendix A.) figure 7 is in effect a measure of the pressure drop per unit thickness across the porous wall, and the abscissa  $(\rho V)_a \frac{\mu_0}{\mu}$  is the reduced weight flow of cooling air per unit of wire-cloth surface area. The viscosity and temperature ratios,  $\mu_{\Omega}/\mu$  and  $(\mu_{\Omega}/\mu)^2~T_{\Omega}/T,$  reduce the air-flow data to NACA standard temperature. A theoretical analysis in reference 8 indicates that the profile of air temperature across a porous wall should practically coincide with profile of metal temperature except for a very short distance on the side the air enters the wall. Consequently, the viscosity- and temperature-ratio factors should be evaluated at the average local wall temperature. Measured wall temperatures on either side of the wire cloth in this afterburner were within 20° R of each other, so for convenience the factors were evaluated at the temperature measured by the air-side thermocouples, which were installed at each station of channels 1 and 9.

The calculated total cooling-air flows in a later section, Cooling-Air Requirements Calculated from Cooling Correlation, were obtained from the step-by-step summation of  $\pi D(\rho V)_a \Delta x$ .

#### Exhaust-Gas Temperature

The total temperature of the exhaust gas was calculated from the exhaust-nozzle total pressure  $P_{68}$ , measured jet thrust, velocity coefficient, and gas flow by the following equation (ref. 7):

$$T_{g,2} = \left(\frac{F_{j,m}}{C_{v}}\right)^{2} \left(\frac{g}{2R}\right) \left(\frac{\gamma_{g}-1}{\gamma_{g}}\right) \left\{\frac{1}{W_{g,68}^{2} \left[1 - \left(\frac{p_{O}}{P_{68}}\right)^{\gamma_{g}}\right]}\right\}$$
(1)

35

The values of R were computed according to the method of reference.9, and the jet velocity coefficient was determined to be 0.97 from data presented in reference 10.

#### Local Combustion-Gas Temperatures

Local values of the combustion-gas total temperature  $T_{g,x}$  with afterburning were computed from the empirical equation (ref. 11)

$$\frac{T_{g,x} - T_{g,1}}{T_{g,2} - T_{g,1}} = \sin \frac{\pi}{2} \frac{x'}{L}$$
 (2)

where  $T_{\rm g,l}$  is assumed equal to the turbine-discharge gas temperature, and  $T_{\rm g,2}$  is the exhaust-gas total temperature. Equation (2) makes no allowance for possible hot streaks and implies a uniform transverse profile of combustion-gas temperature. Hot streaks undoubtedly were present, although observation of the combustion color and pattern by means of a periscope directed up the burner axis showed good circumferential uniformity. The transverse temperature profile was made as uniform as possible in a previous investigation of the radial fuel-air distribution when this same configuration had a convection-cooled impermeable wall.

For nonafterburning cooling data, local values of bulk total temperature  $T_{\rm g,x}$  were assumed equal to the turbine-discharge gas temperature  $T_{\rm g,1}$ .

#### Correlation of Cooling Data

Cooling data from five stations along the two typical channels of wire cloth were correlated by plotting the temperature-difference ratio  $(T_w - T_a)/(T_g - T_a)$  against the coolant-flow ratio  $(\rho V)_a/(\rho U)_g$  for constant values of bulk Reynolds number. The flow over the porous wall was believed to be similar to the boundary-layer flow over a flat plate, so that the length used in the Reynolds number was taken as the distance from the leading edge of the porous wall. Consequently, the temperature-difference ratios and the coolant-flow ratios are local values corresponding to the local Reynolds numbers. The viscosity of the combustion gas was assumed to be the same as for air given in table 2 of reference 12 and was evaluated at the film temperature  $T_f$ . The quantity  $(\rho U)_g$  was assumed identical to the local one-dimensional value of total weight flow per unit of combustion-chamber flow area.

The wall temperature  $T_w$  in the temperature-difference ratio  $(T_w - T_a)/(T_g - T_a)$  was measured on the cooling-air side of the wire cloth but can be considered practically to represent the wall temperature on the hot-gas side because of the small difference in measured temperatures across the wire cloth in this afterburner.

Cooling-Air Requirements Calculated from Cooling Correlation

The experimental cooling correlation of this investigation was used to calculate the longitudinal profile of porous-wall temperature in this afterburner. The conditions analyzed are given in the following table:

Flight condition	Flight Mach number	Altitude, ft	Exhaust-gas total temperature, T <sub>g,2</sub> ,
A B B C	0 .8 .8 1.5 2.0	Sea level 35,000 35,000 35,000 35,000	3700 3700 3200 3700 3700

The turbine-discharge temperature was 1710° R for all conditions. The cooling-air static pressure and the permeability of the porous wall were assumed to be absolutely uniform, and the air-flow calibration of the porous wall was assumed to be identical with the mean calibration curve of figure 7. With a uniform permeability, most of the porous wall will be overcooled except for some peak temperature region, which must not exceed the maximum allowable operating temperature of the porous material. The calculated maximum wall temperatures were plotted against total flow ratio for each flight condition. It should be kept in mind that wall temperatures calculated from the cooling correlation are assumed to be uniform around the circumference at each station. Usually, a safety factor must be allowed for random hot spots in the porous wall caused by hot streaks in the combustion—gas—or—by—local—areas\_that\_have\_less than the mean permeability.

Minimum cooling-air flow. - The minimum cooling-air flow for a given temperature limit results when the wall temperature is maintained constant at the maximum allowable operating temperature of the porous material by use of an infinitely variable permeability distribution along the porous wall. The assumption of a constant wall temperature makes it possible to compute the minimum cooling-air distribution and the minimum total flow ratio directly from the cooling correlation without considering the distributions of permeability that would be

required to provide the minimum cooling-air distribution. Although it is not practical to vary the permeability distribution for each flight and operating condition in an actual afterburner, the minimum flow ratios are useful for reference and for examination of trends. Minimum total flow ratios were therefore also computed for flight conditions A to D with a constant porous-wall temperature of  $1210^{\circ}$  R.

Longitudinal profile of combustion-gas static pressure. - The static-pressure profile along the length of the combustion chamber was calculated step-by-step from well-known one-dimensional flow relations for momentum pressure drop in a constant-area duct and the isentropic variation of Mach number with area ratio. The friction pressure drop, which was assumed to be small relative to the momentum pressure loss, was neglected.

Cooling-air pressure and temperature. - The cooling air was assumed to have been bled from an interstage of the compressor (at a compressor efficiency of 0.85) at a pressure high enough to allow for a pressure drop of 1 pound per square inch through valves and ducting to the upstream edge of the porous wall. The pressure drop across the porous wall was limited to a minimum of 1 pound per square inch for practical control, and to a maximum of 6 pounds per square inch to prevent bursting the channels of wire cloth. The cooling-air pressure and temperature were presumed to be uniform in all cooling-air passages. Convective heat transfer to the cooling air by the impermeable wall upstream of the porous wall was assumed to raise the air temperature  $50^{\circ}$  above that corresponding to the compressor bleed temperature.

Cooling-Air Requirements with Forced-Convection Cooling

Cooling-air requirements for forced-convection cooling of this afterburner with ram air were calculated for exhaust-gas temperatures of  $3200^{\circ}$  and  $3700^{\circ}$  R for flight condition B from data in reference 13 and the cooling correlation of reference 11.

#### RESULTS AND DISCUSSION

#### Typical Data

Figure 8 shows typical measured circumferential profiles of the cooling-air static pressure and wire-cloth temperature. The static-pressure profiles shown result from the tangential inlet on the plenum chamber and the previously mentioned order of assembling the channels of wire cloth. As would be expected, the temperature profiles are the reverse of the pressure profiles. Figure 8 shows that channel 1 was generally the hottest and channel 9 the coldest, with or without afterburning.

Typical longitudinal profiles for the wire-cloth afterburner are shown in figure 9. The importance of eliminating circumferential gradients in cooling-air static pressure and in permeability is obvious from the 530°R variation in wall temperature at station 62 in figure 9(a). Part of the circumferential temperature spread in this afterburner would have been averted if there had been no circumferential pressure gradient in the cooling air. The pressure gradient could have been reduced by a better plenum-chamber inlet or by cross-flow holes in the angles that supported the channels of wire cloth. Wire cloth more closely meeting the specified permeability could have practically eliminated circumferential variations in wall temperature, except for those caused by any hot streaks in the combustion gas. The slight drop in cooling-air temperature (figs. 9(a) and (c)) along the length of the cooling-air passage is due to heat losses through the uninsulated shroud.

The longitudinal profiles of static pressures on both sides of the porous wall are shown at the top of figures 9(b) and (d). For the relatively high flow ratios shown ( $W_a/W_g$  of 0.0716 to 0.0951), the continuous bleeding of air through the porous wall caused a deceleration of the cooling-air flow and a corresponding rise in static pressure of the cooling air in the flow direction. With the low flow ratios of practical interest, the static pressure of the cooling air was almost independent of passage length.

The variation of pressure drop across the porous wall with distance along the wall is represented by the vertical distance between the static pressures of the cooling air and of the combustion gas. The resulting longitudinal profiles of coolant-flow ratio (pV) a/(pU) g figures 9(b) and (d). The coolant-flow ratios for channel 9 were considerably higher than for channel 1. The differences in coolant-flow ratios are caused by the differences in permeability and the absolute pressure level in each channel. It is recalled that the air-flow calibrations of figure 7 indicate  $(\rho V)_a$  is a function of the difference of the squares of the absolute static pressure on both sides of the porous wall instead of the pressure drop alone. The curves of the fraction of total cooling-air flow in each channel are almost linear and nearly identical for channels 1 and 9 (figs. 9(b) and (d)). It can be inferred, therefore, that the longitudinal addition of cooling air was almost linear through all the channels of wire cloth.

Before discussing the cooling correlation, it is of interest to determine whether there was any progressive change in the air-flow calibration of the wire cloth during the cooling investigation. A dull greasy smudge formed on the combustion-gas side of the wire cloth in spite of the cooling-air film flowing away from the wire cloth during all periods of engine operation. The smudge is visible in figure 10 to the left of the white lines. The areas to the right of the white lines have

been wiped clean with cleansing tissue to show the condition of the wire cloth after 4 hours 10 minutes of afterburning. The smudge caused no discernible effect on air-flow calibration.

Figure 11 shows the circumferential average static-pressure drop across the porous wall against orifice cooling-air flow for several levels of combustion-chamber pressure at stations 24 and 57.5. The agreement between data taken before and during the cooling investigation was excellent at all stations. On the basis of figure 11 and the close agreement between temperature-difference ratios for nonafterburning check points, it is concluded that there was no significant change in the air-flow calibration of the wire cloth during the cooling investigation.

#### Cooling Correlation

The experimental cooling data with afterburning are correlated over a range of Reynolds numbers in figures 12(a) to (f). Cooling data obtained from channels 1 (hottest) and 9 (coldest) met, or overlapped, to define a single curve when the Reynolds number was held approximately constant. The mean curves drawn through groups of data points having approximately the same Reynolds number are summarized in figure 12(g). Within the ranges investigated, neither Reynolds number nor radiation had any marked effect on the correlation of afterburning cooling data for coolant-flow ratios less than about 0.007. Above a coolant-flow ratio of 0.007, the temperature-difference ratio, and hence the porouswall temperature for fixed cooling-air and gas temperatures, decreased as Reynolds number increased from about 75,000 to 800,000. The curves for Reynolds numbers of 1,000,000 and 1,500,000 lie, respectively, above and below the curve for 800,000. It is probable that in this Reynolds number range, corresponding to stations 49.6 and 57.5, increases in radiant heat transfer tend to counterbalance increases in the Reynolds number (see ref. 1), although the radiant heat transfer was calculated to be less than one-tenth of the convective heat transfer.

A direct comparison between the curves of the experimental cooling correlation and those predicted by the approximate theory of references 4 and 5 is not entirely realistic because of the different assumptions used with these data and those used for developing the approximate theory. However, a partial comparison is made in appendix B.

Although nonafterburning conditions were not of primary importance to the present investigation, the nonafterburning conditions are of somewhat general interest in connection with the heat-transfer process of transpiration cooling. The combustion-gas temperature was almost constant along the length of the combustion chamber during nonafter-burning, and radiation from the gas was negligible because of the low

gas temperature and pressures. The nonafterburning cooling data are presented in tables I to IV. Nonafterburning cooling data are shown in figure 13 by plotting  $(T_w - T_a)/(T_g - T_a)$  against Reynolds number for constant values of  $(\rho V)_a/(\rho U)_g$ . Cooling correlation curves for Reynolds numbers of  $10^5$  and  $10^6$  (fig. 14) were obtained from a cross plot of figure 13. The curves of figure 14 are similar in shape and magnitude to the afterburning data for comparable Reynolds numbers, as can be seen in figure 15. Although somewhat better cooling is indicated by the nonafterburning than by the afterburning data at coolant-flow ratios less than about 0.007, the agreement between afterburning and nonafterburning data is considered satisfactory. The agreement probably would have been closer if measured values had been available of the local combustion-gas temperatures and of  $(\rho U)_g$  near the wall, instead of assuming  $(\rho U)_g = W_g/A_g$ . The profiles of  $(\rho U)_g$  are known to

#### Transpiration-Cooling Performance

differ between nonafterburning and afterburning conditions.

Figure 16 is a plot of the calculated maximum wall temperature against total flow ratio  $W_a/W_g$  for the assumed flight conditions A to D when operating with an exhaust-gas temperature of  $3700^{\circ}$  R. It should be emphasized that the air flow through the porous wall is a function of the difference of the squares of the absolute pressures on either side of the wall (see fig. 7). Hence the magnitude and the longitudinal position of the maximum wall temperature are functions of the profiles of the absolute static pressures and of the combustion-gas temperature. The profiles of absolute static pressure are dependent on the flight condition and the pumping characteristics of the engine used, in addition to pressure losses in the afterburner. For the flight conditions investigated, the maximum wall temperature occurred at the leading edge of the porous wall, except when the cooling-air static pressure was reduced to 10.85 pounds per square inch absolute. At this pressure, the maximum wall temperature moved to about station 49.6.

Separate-curves-of-maximum-wall-temperature-against-total-flow-ratio-were obtained for each flight condition (fig. 16). The curves closely overlap so that the cooling-air requirements were nearly independent of flight conditions; however, the curves would be separated more if the gas temperature had been widely varied. The operable range of total flow ratio varied with flight condition because of the related minimum and maximum pressure drops across the porous wall. The upper symbol on each curve corresponds to the assumed minimum pressure drop across the porous wall of 1 pound per square inch at the leading edge. The lower symbol corresponds to the assumed maximum pressure drop of 6 pounds per square inch at the trailing edge. The resulting minimum and maximum cooling-air pressures are given in figure 16. With a uniform distribution of cooling-air pressure,

the range in static pressure for control of cooling-air flow at a given flight condition is then 5 pounds per square inch minus the drop in combustion-chamber static pressure along the porous wall. Consequently, large drops in combustion-chamber pressure along the porous wall tend to decrease the range of cooling-air static pressure for control of cooling-air flow. The control range for cooling-air static pressure varied from 3.70 to 0.66 pounds per square inch, respectively, for flight conditions B and D. Cooling-air pressure must be accurately controlled within this range. For example, at flight condition D, a decrease in cooling-air static pressure of 0.66 pound per square inch (only 1.85 percent of the absolute cooling-air pressure) causes a 256° R increase in maximum wall temperature.

Greater range could be obtained in cooling-air static pressure by using several layers of wire cloth. This type of construction would permit higher pressure drops across the porous wall and would make possible the control of low flows corresponding to high maximum wall temperatures without danger of reverse flow through the wall. The peak temperature limit for the porous wall was about 14100 R because of oxidation of the brazing alloy on the wire cloth in this afterburner. Therefore, a temperature of 1210° R is assumed to be safe for the maximum wall temperatures computed from the cooling correlation. This temperature provides a 200° safety factor for local peak temperatures caused by hot streaks in the combustion gas and from small random areas of the cloth that have less than the mean permeability. A total flow ratio  $W_{\rm a}/W_{\rm g}$  of about 0.032 can maintain a maximum wall temperature of 1210° R with an exhaust-gas temperature of 3700° R at conditions A to C. Calculations indicated that a maximum wall temperature of 1210° R could also be maintained at condition D by increasing the assumed maximum allowable pressure drop across the wire cloth by about 20 percent (point indicated by the end of the dotted extension). A visual extrapolation of the curves of figure 16 (disregarding pressure limits) to a wire-cloth temperature of 1760° R, which is a representative temperature for a wall of stainless steel, results in a total flow ratio of about 0.018. This value compares favorably with the total flow ratio of 0.016 computed in reference 2 for the same maximum wall temperature with a porous wall of sintered stainless steel and an exhaust-gas temperature of about 3800° R. The somewhat more effective cooling indicated for a porous wall of sintered stainless steel in reference 2 may be caused by a more uniform film of cooling air on the sintered wall than that produced by the fewer number of larger pores in the surface of the wire cloth.

A total flow ratio of 0.032 for flight conditions A to D when using a uniform permeability distribution is about 15 percent higher than the minimum total flow ratio for a constant wall temperature of  $1210^{\circ}$  R which would generally require a different permeability distribution for each flight condition. Therefore, the practicability of

using wire cloth having a nonuniform longitudinal distribution of permeability, compromising the variable permeability distributions required to maintain a constant wall temperature for each of the flight conditions investigated, is questionable.

Some reductions should be expected in the total flow ratios of transpiration-cooled afterburners if, through quality control, the tolerance on the uniformity of permeability can be decreased from that of the brazed and rolled wire cloth used. The use of porous materials having sufficient strength and resistance to oxidation at higher operating temperatures will also permit a reduction in cooling-air flow. For example, the minimum total flow ratio would decrease about 49 percent if the maximum wall temperature could be increased from 1210° to 1760° R, which may be possible for cloth woven from stainless steel or Inconel wires. It is expected that problems due to oxidation of a braze alloy can be solved by the use of high-temperature brazing alloys under development, or by the substitution of sintering for brazing.

Comparison of Transpiration and Forced-Convection Cooling

The cooling-air requirements for transpiration and forced-convection cooling of this afterburner are compared in figure 17 for exhaust-gas temperatures of 3200° and 3700° R at flight condition B. A typical maximum wall temperature for a forced-convection-cooled wall of stainless steel is 1760° R. With a maximum wall temperature of 1210° R, or limited by minimum practical pressure drop, for a transpiration-cooled wall of brazed and rolled wire cloth, the total flow ratios with transpiration cooling are about 16 percent of the convective requirements for exhaust-gas temperatures of 3200° and 3700° R. The corresponding inlet cooling-air temperatures are shown at the top of the figure to be about 635° and 444° R, respectively, for transpiration and forced-convection cooling. The higher temperature with transpiration cooling results from compressor bleed and from heat absorbed in convectively cooling the impermeable wall upstream of the porous wall.

#### Pressure Environment of Wire Cloth

The wire cloth successfully withstood the pressure surges of six afterburner starts and the usual pulsations in pressure during normal steady-state afterburning. Ignition of the afterburner usually caused surges in combustion-chamber static pressure to peak values of 2 to 5 inches of mercury. The surges damped out in less than 1 second to the steady-state values. The surge in combustion-chamber static pressure caused similar surges in cooling-air static pressure that varied anywhere from 0.2 to 1.0 or 1.5 inches of mercury. These surges dissipated to steady-state values in several seconds. During steady-state operation

both the cooling-air and combustion-chamber pressure traces showed background pressure pulsations of 100 cps with a total amplitude of about 0.10 to 0.15 inch of mercury superimposed with peaks up to about 1 or 2 inches of mercury total amplitude at roughly 3 cps. The duration of these peaks was about 0.01 second. In one or two instances beats were observed in the trace of combustion-chamber static pressure at a beat frequency of 7 cps with a total amplitude of about 1 to 2 inches of mercury.

#### CONCLUDING REMARKS

Cooling data were obtained for a transpiration-cooled afterburner having a porous combustion-chamber wall of brazed and rolled wire cloth. The data cover a range of exhaust-gas temperature from 1200° to 3340° R, total flow ratio of cooling air to combustion gas of 0.025 to 0.106, and pressure altitudes of 15,000 to 45,000 feet. The data are successfully correlated over a range of Reynolds numbers from 75,000 to 1,500,000 based on the distance downstream of the leading edge of the porous wall.

Maximum wall temperatures, based on the cooling correlation, were determined for a porous wall of uniform permeability at sea-level take-off and for flight Mach numbers of 0.8, 1.5, and 2.0 at an altitude of 35,000 feet. The cooling-air requirements were nearly independent of the flight conditions. A total flow ratio of cooling air to combustion gas of about 0.032 can maintain a maximum wall temperature of 1210° R with an exhaustgas temperature of 3700° R. Savings in cooling air would, of course, be possible with porous material having a higher allowable maximum wall temperature.

The total flow ratios with a uniform permeability distribution and air flows sufficient to limit the maximum wall temperature to  $1210^{\circ}$  R are about 15 percent higher than the minimum total flow ratios corresponding to a variable-permeability wall with a constant wall temperature of  $1210^{\circ}$  R.

The total flow ratios of cooling air to combustion gas for a maximum wall temperature of  $1210^{\circ}$  R with the wire-cloth afterburner are about 16 percent of the total flow ratios required to convectively cool a stainless-steel afterburner wall to a maximum temperature of  $1760^{\circ}$  R with exhaust-gas temperatures of  $3200^{\circ}$  and  $3700^{\circ}$  R.

The analysis of cooling-air requirements for the previously mentioned flight conditions indicated that cooling-air static pressure must be closely controlled, especially at a flight Mach number of 2.0.

Lewis Flight Propulsion Laboratory
National Advisory Committee for Aeronautics
Cleveland, Ohio, June 11, 1954

#### APPENDIX A

#### SYMBOLS

The following symbols are used in this report:

$A_{\mathbf{g}}^{\prime}$	combustion-chamber flow area, sq in.
C <sub>v</sub>	<pre>jet velocity coefficient, measured jet thrust   divided by isentropic jet thrust for measured   mass flow</pre>
c p	specific heat at constant pressure
D	inside diameter of combustion chamber, in.
<sup>F</sup> j,m	measured jet thrust, 1b
g	acceleration due to gravity, $ft/sec^2$
Hg,c	convective heat-transfer coefficient that would apply to a solid surface under identical outside flow conditions, Btu/(sec)(sq in.)(OR)
Hg,r	coefficient of nonluminous heat transfer, Btu/(sec)(sq in.)(OR)
K	permeability coefficient, sq in. (defined in eq. (6) of ref. 3)
L ·	distance from flame holder to exhaust-nozzle exit, 66 in.
Nu	Nusselt number
Р	total pressure, lb/sq in. abs
Pr	Prandtl number
р	static pressure, lb/sq in. abs
Δ(p <sup>2</sup> )	difference between squares of absolute static pressures on both sides of porous wall, $p_a^2$ - $p_g^2$ , $1b^2/in^4$
$\log_{10} \left[ \frac{\Delta(p^2)}{\tau} \left( \frac{\mu_0}{\mu_0} \right)^2 \frac{T_0}{T} \right]$	pressure-drop parameter, $1b^2/in.^5$

```
gas constant, ft-lb/(lb)(OR)
R
              Reynolds number, (\rho U)_g(x - 21)/\mu_f
Re
              total temperature of a gas or surface temperature of a
Т
                 solid, OR
              film temperature, \frac{T_g + T_w}{2}, o_R
T_{f}
              total temperature at combustion-chamber inlet, OR
T_{g,1}
              total temperature of exhaust gas at nozzle exit, OR
Tg,2
              NACA standard sea-level temperature, 518.4° R
T_{O}
\frac{T_{w} - T_{a}}{T_{g} - T_{a}}
              temperature-difference ratio
              velocity in axial-flow direction, in /sec
U
              velocity normal to porous-wall surface, in./sec
              weight flow, lb/sec
Wa/Wg
              total flow ratio
              distance downstream of quick-disconnect coupling at
х
                combustion-chamber inlet, in.
x 1
              distance downstream of flame holder, x - 2, in.
              incremental length of combustion chamber, in.
Δх
              absorptivity of combustion gas
\alpha_g
              ratio of specific heats of exhaust gas
\gamma_{\rm g}
              emissivity
              absolute viscosity, lb/(in.)(sec)
μ
              weight density, lb/cu in.
              total weight flow per unit of combustion-chamber flow area,
                \left(W_{g} + \sum_{n=1}^{\infty} W_{a}\right) / A_{g,x}, lb/(sec)(sq in.)
```

```
(\rho V)_{a}\mu_{O}/\mu reduced weight flow per unit area, lb/(sec)(sq~in.)
```

 $(\rho V)_g/(\rho U)_g$  coolant-flow ratio

thickness of wire cloth, in.

Subscripts:

a cooling air

f refers to property evaluated at film temperature  $T_{\mathbf{f}}$ 

g combustion gas

w wall

x at distance x

O free-stream conditions

Numbers greater than 2 represent stations along combustion chamber in inches downstream of quick-disconnect coupling.

#### APPENDIX B

#### COMPARISON OF EXPERIMENTAL COOLING CORRELATION WITH THEORY

A brief comparison is made between the experimental cooling correlation and the approximate theory of Rannie and Friedman (refs. 4 and 5) for turbulent boundary-layer flow. The comparison is made between the temperature-difference ratio for individual data points and the theoretical temperature-difference ratio corresponding to the same experimental conditions.

The theoretical equation is given by Friedman (ref. 5) as

$$\frac{T_V - T_a}{T_g - T_a} = \frac{r}{e^{r\phi} + r - 1}$$
 (B1)

where r is the ratio of the velocity parallel to the surface at the border between the laminar sublayer and the turbulent part of the boundary layer to the stream velocity outside the boundary layer. Eckert (ref. 14) gives

$$r = \frac{2.11}{(Re)_g^{0.1}}$$
 (B2)

$$\Phi = \frac{(\rho V)_a c_{p,a}}{H_{g,c}}$$
 (B3)

For turbulent boundary-layer flow over a flat plate, Colburn gives

$$Nu = 0.0296(Re)^{0.8}(Pr)^{1/3}$$
 (B4)

where Re is based on the distance from the leading edge. Rearranging equation (B4) gives

$$\frac{\text{Nu}}{\text{RePr}} = \frac{\text{Hg,c}}{(\rho U)_{g} c_{p,g}} = \frac{0.0296}{(\text{Re})^{0.2} (\text{Pr})^{2/3}}$$
(B5)

from which the local value of convective heat-transfer coefficient at any station  $\mathbf{x}$  is

$$H_{g,c,x} = \frac{0.0296(\rho U c_p)_{g,x}}{(Re)_{g,x}^{0.2}(Pr)_{g,x}^{2/3}}$$
(B6)

The effect of temperature level on the Prandtl number is so small that a mean value was used for all cases.

The effects of nonluminous radiation were accounted for by substituting the sum of the equations (B6) and (B7) for  $H_{g,c}$  in equation (B3). From the data of reference 15,

$$H_{g,r,x} = \frac{0.173 \epsilon_{s}'}{(144)(3600)(T_{g,x}-T_{w,x})} \left[ \epsilon_{g,x} \left( \frac{T_{g,x}}{100} \right)^{4} - \alpha_{g,x} \left( \frac{T_{w,x}}{100} \right)^{4} \right]$$
(B7)

where  $H_{g,r,x}$  is the heat-transfer coefficient for nonluminous radiation at station x. A value of 0.52 was used for the pseudoemissivity  $\epsilon_{:}$ . The local values of combustion-gas emissivity  $\epsilon_{g,x}$  and absorptivity  $\alpha_{g,x}$  were based on the total fuel-air ratio and local one-dimensional values of temperature and static pressure. No distinction was made between total and static combustion-gas temperature, because the Mach numbers in the combustion chamber were low.

The density and viscosity in the Reynolds number in equation (B6) are usually based on the gas temperature just outside the boundary layer. However, in order to obtain a better correlation of heat-transfer data over a large range of  $T_{\rm w}/T_{\rm g}$ , the combination of equations (B3) and (B6) (ignoring radiation) was modified in reference 16 to

$$\Phi = \frac{(\text{Re})^{0.2}(\text{Pr})^{2/3}}{0.0296} \frac{(\rho V)_a}{(\rho U)_g} \frac{T_w}{T_g}$$
 (B8)

The temperature ratio  $T_{\rm w}/T_{\rm g}$  has the effect of evaluating the density and viscosity in the Reynolds number at the wall temperature.

In view of equation (B8), the following equation was derived for  $\phi_{\rm X}$ :

$$\phi_{x} = \frac{T_{w,x}}{T_{g,x}} \frac{(\rho V c_{p})_{g,x}}{\frac{0.0296(\rho U c_{p})_{g,x}}{(Re)_{g,x}^{0.2/3}} + \frac{0.173 \epsilon'_{s}}{\frac{(144)(3600)(T_{g,x}-T_{w,x})}{(T_{g,x}-T_{w,x})}} \left[\epsilon_{g,x} \left(\frac{T_{g,x}}{100}\right)^{4} - \alpha_{g,x} \left(\frac{T_{w,x}}{100}\right)^{4}\right]}$$
(B9)

Equation (B9) was used in equation (B1) and found to overcorrect the theoretical temperature-difference ratio, so that the intermediate temperature ratio  $T_{\rm w,x}/T_{\rm f,x}$  was used in the comparison figures 18 and 19. With afterburning, the inclusion of  $T_{\rm w,x}/T_{\rm f,x}$  in equation (B9) results in theoretical wall temperatures generally higher (fig. 18(a)) than those measured. When a value of 1 is assumed for  $T_{\rm w,x}/T_{\rm f,x}$ , the theoretical wall temperatures are lower than those measured and the scatter is less (fig. 18(b)).

For the nonafterburning data, the inclusion of  $T_{w,x}/T_{f,x}$  in equation (B9) results in theoretical wall temperatures that are equal to or slightly lower than those measured (fig. 19(a)). The assumption of  $T_{w,x}/T_{f,x}$  of l results in a slight lowering of the theoretical wall temperatures over the entire range of temperature-difference ratio (fig. 19(b)).

The determination of an empirical coefficient or exponent for  $T_{w,x}/T_{f,x}$  to produce a better agreement does not appear warranted because of differences in the assumptions made in the theory and conditions in the afterburner. Therefore, no conclusion is made as to the validity of including the temperature ratios  $T_{w,x}/T_{f,x}$  or  $T_{w,x}/T_{g,x}$  in the equation for  $\phi$ .

#### REFERENCES

- 1. Eckert, E. R. G., and Livingood, John N. B.: Comparison of Effectiveness of Convection-, Transpiration-, and Film-Cooling Methods with Air as Coolant. NACA TN 3010, 1953.
- 2. Koffel, William K.: Preliminary Experimental Investigation of Transpiration Cooling for an Afterburner with a Sintered, Porous Stainless-Steel Combustion-Chamber Wall. NACA RM E53D08, 1953.
- 3. Koffel, William K.: Air-Flow Characteristics of Brazed and Rolled Wire Filter Cloth for Transpiration-Cooled Afterburners. NACA RM E53H24, 1953.
- 4. Rannie, W. D.: A Simplified Theory of Porous Wall Cooling. Prog. Rep. 4-50, Power Plant Lab. Proj. No. MX801, Jet Prop. Lab., C.I.T. Nov. 24, 1947. (AMC Contract No. W-535-ac-20260, Ord. Dept. Contract No. W-04-200-ORD-455.)
- 5. Friedman, Joseph: A Theoretical and Experimental Investigation of Rocket-Motor Sweat Cooling. Jour. Am. Rocket Soc., no. 79, Dec. 1949, pp. 147-154.

- 6. Huntley, S. C., Auble, Carmon M., and Useller, James W.: Altitude Performance Investigation of a High-Temperature Afterburner. NACA RM E53D22, 1953.
- 7. Conrad, E. William, and Campbell, Carl E.: Altitude Wind Tunnel Investigation of High-Temperature Afterburners. NACA RM E51L07, 1952.
- 8. Weinbaum, S., and Wheeler, H. L., Jr.: Heat Transfer in Sweat-Cooled Porous Metals. Prog. Rep. 1-58, Air Lab. Proj. No. MX121, Jet Prop. Lab., C.I.T., Apr. 8, 1947. (AMC Contract No. W-535-ac-20260, Ord. Dept. Contract No. W-04-200-ORD-455.)
- 9. Pinkel, Benjamin, and Turner, L. Richard: Thermodynamic Data for the Computation of the Performance of Exhaust-Gas Turbines. NACA WR E-23, 1944. (Supersedes NACA ARR 4B25.)
- 10. Wallner, Lewis E., and Wintler, John T.: Experimental Investigation of Typical Constant- and Variable-Area Exhaust Nozzles and Effects on Axial-Flow Turbojet-Engine Performance. NACA RM E51D19, 1951.
- ll. Koffel, William K., and Kaufman, Harold R.: Empirical Cooling Correlation for an Experimental Afterburner with an Annular Cooling Passage. NACA RM E52Cl3, 1952.
- 12. Keenan, Joseph H., and Kaye, Joseph: Gas Tables. John Wiley & Sons, Inc., 1948.
- 13. Koffel, William K., and Kaufman, Harold R.: Cooling Characteristics of an Experimental Tail-Pipe Burner with an Annular Cooling-Air Passage. NACA RM E51K23, 1952.
- 14. Eckert, E. R. G.: Introduction to the Transfer of Heat and Mass. McGraw-Hill Book Co., Inc., 1950.
- 15. McAdams, William H.: Heat Transmission. Second ed., McGraw-Hill Book Co., Inc., 1942, pp. 64-69.
- 16. Esgar, Jack B.: An Analytical Method for Evaluating Factors
  Affecting Application of Transpiration Cooling to Gas Turbine
  Blades. NACA RM E52GO1, 1952.

TABLE I. - FLIGHT AND OPERATING CONDITIONS

Exhaust- gas total temper- ature, Gg,						2583 2767 2594 2784 1826 2696	2714 2527 2626 2477 295 <b>6</b> 3013	2384 2831	2612	1801 1832 2739 2717 2820	2744 3042 2954 2963 2963	2913 3104 3120 3216 3340	3176 3198
Turbine- outlet total pres- sure, 1b/sq ft	-	2040 2034 2044 2029 2043	1159 1154 1160 1159 1155	1158 1155 1171 1156 1162		2470 2454 2475 2482 2725	2613 2703 2743 2752 2916 2957 2998	2032	1967	1218 1213 1393 1385 1430	1415 1517 1495 1500 1513	1522 1523 1524 1554 1554	967 941
Turbine- outlet gas total tempera- ture, OR		1203 1203 1203 1203 1204 1204	1241 1247 1251 1249 1251	1249 1256 1204 1249 1249		1384 1379 1377 1391 1331	1371 1329 1350 1362 1417 1433	1 <b>547</b> 1470	1487	1280 1284 1438 1421 1467	1453 1534 1521 1535 1525	1551 1557 1550 1592 1627	1663 1653
Cooling- air inlet total tempera- ture, T		535 535 535 535 535 535	535 535 532 535 535 535	528 533 531 537 533 534		539 539 537 537 537	537 537 537 537 537	536 536	535	529 529 540 540	533 533 533 533	532 536 536 536 536	540
Total flow ratio, Wa/W	,	0.0253 .0298 .0447 .0595 .0761	0.0310 .0406 .0426 .0485 .0492	.0504 .0515 .0513 .0530 .0764		0.0511 .0500 .0564 .0280 .0602	.0551 .0483 .0527 .0527 .0535	0.0692	0.0857	0.1059 .0975 .0595 .0456	.0688 .0716 .0803	.0973 .0792 .0716 .0769	0.1007
Cooling- air flow, Wa		1.201 1.417 2.172 2.922 3.827	0.828 1.092 1.29 1.317 1.328	1.35 1.392 1.412 2.141 2.704		2.570 2.433 2.861 1.3660 3.10 2.68	3.13 2.71 2.96 3.09 3.08	3.015	3.168	3.16 2.87 1.67 1.26 2.21	1.95 2.601 2.068 2.332 2.623	2.896 2.29 2.23 2.23	1.79
After- burner fuel flow,			00000	00000		5170 5170 5170 5192 5950 6175	6175 6448 6488 6488 6535 6715	4150	3807	2770 2865 3050 3050 3050	3055 3230 3260 3260 3260	3260 3605 3655 3805 4186	2230 2230
Engine fuel flow, lb/hr	<b>8</b> t	1590 1601 1601 1601 1601 1601	1050 1057 1056 1036 1050 1045	1070 1055 1073 1050 1060		1929 1918 1929 1940 2218 2287	2310 2211 2242 2248 2440 2502	1612 1812	1582	1102 1091 1197 1180 1238	1213 1329 1320 1320 1320	1345 1322 1322 1380 1413	957 930
Engine- inlet air flow, lb/sec	Nonafterburning	45.77 45.74 45.95 45.99 45.99	25.57 25.52 25.53 25.53 25.53	25.46 25.37 25.37 25.54 25.57	Afterburning	45.71 45.71 45.94 45.46 51.51 51.51	51.35 50.77 50.85 50.85 51.41 51.43	38.94	32.28	25.60 25.48 25.28 25.28 25.28	25.30 25.41 25.55 25.52 25.70	25.57 25.31 25.38 25.31 25.15	15.71
Engine- inlet total pres- sure, lb/sq ft	Nona	1699 1700 1700 1700 1701	946 947 1021 942 942 1005	99999999999999999	Aft	1710 1710 1715 1700 1705	1707 1703 1700 1700 1707 1707	1445	1200	948 941 953 953	953 970 938 945	99999999999999999999999999999999999999	601 591
Engine- inlet air temper- ature,		50000000000000000000000000000000000000	535 535 536 532 535 535	535 535 527 537 534		540 540 540 540 456	4 4 4 4 4 4 4 4 4 4 4 4 6 5 5 5 5 5 5 5	538	537	534 534 540 540 537	539 536 530 529	530 536 536 536	540
After- burner fuel-air ratio at exhaust nozzle						0.036 .035 .035 .037 .0365	0383 0403 0406 0406 0421	0.033	0.037	0.03205 .03364 .0353 .0359	.0349 .040 .041 .041	.040 .0431 .0438 .0487	0.0464
Engine speed, rpm		12,478 12,496 12,496 12,486 12,486 12,489	12,502 12,505 12,464 12,496 12,496 12,508	12,499 12,505 12,519 12,492 12,502		12,508 12,499 12,503 12,487 12,531	12,503 12,515 12,489 12,489 12,447 12,484	12,499	12,511	12,528 12,541 12,508 12,514 12,486	12,508 12,496 12,546 12,515	12,509 12,505 12,496 12,515 12,515	12,521
Flight Mach number			000000	000000		7.0	riririr	0.63	0.74	00000	00000	000001	0.01
Altitude pressure, PO, lb/sq ft abs		1193 1200 1193 1193 1195	500 498 512 500 498 498	501 508 508 520 497 494		1202 1195 1195 1175 1206	1211 1201 1197 1204 1204 1204	1108	835	512 492 504 508 509	508 500 500 500	508 504 504 508	318 321
Altitude,		15,000	35,000			15,000		16,500	23,500	35,000			45,000
Series and run		127-27 127-26 127-25 127-24 127-23	127-21 127-20 130-17 127-22 130-24	128-4 129-18 129-7 129-32 127-18		129-25 129-26 129-24 129-23 130-37	130-33 130-31 130-29 130-29 130-34	129-21	129+20	128-5 128-6 130-20 130-21 130-18	130-19 129-19 129-11 129-10	129-9 130-27 130-28 130-26 130-25	130-22 130-23

TABLE II. - COMBUSTION-CHAMBER WALL TEMPERATURES, OF

Series and run		Solid wal			Wire-cl	oth por	rous wal	L 
		<sup>T</sup> w,10	<sup>T</sup> w,19	Tw,24	Tw,32.6	Tw,41	Tw,49.6	Tw,57.5
127-27	1	558	553	429	459	<b>443</b>	419	400
	9	588	530	459	422	<b>3</b> 66	323	358
127-26	1	5 <b>43</b>	5 <b>33</b>	412	<b>4</b> 22	410	389	370
	9	570	512	420	<b>3</b> 82	331	293	330
127-25	1	499	489	348	338	326	310	300
	9	524	464	338	292	254	231	265
127-24	1 9	468 . 490	449 429	302 283	282 239	270 210	260 193	250 220
127-23	1	429	411	26 <b>8</b>	2 <b>4</b> 0	228	213	212
	9	452	392	240	198	183	160	181
127-28	1	428	409	269	2 <b>4</b> 0	229	219	213
	9	451	393	2 <b>4</b> 0	198	186	160	182
127-21	1	600	549	437	462	460	<b>434</b>	422
	9	610	5 <b>34</b>	422	388	346	312	339
127-20	1	567	518	394	407	406	379	362
	9	583	<b>4</b> 99	372	331	293	263	287
130-17	1	557	514	372	355	<b>34</b> 7	321	322
	9	568	489	338	302	287	252	273
12717	1	538	503	367	372	368	339	<b>333</b>
	9	568	482	3 <b>3</b> 8	295	261	236	256
127-22	1	544	500	367	373	365	343	332
	9	568	481	337	294	260	219	265
130-24	. 1	569	518	376	364	. <b>354</b>	330	330
	. 9	576	493	347	310	289	262	282
128-4	—-1—-	-839-	-815	810	7.25	780	745	850
	9	686	802	719	677	762	885	823.
129-18	1	542	509	371	360	348	329	32 <b>4</b>
	9	370	482	338	298	279	242	267
129-7	1	532	496	366	<b>3</b> 53	<b>34</b> 2	325	<b>3</b> 22
	9	558	473	326	288	259	237	259
129-32	1 ·	539	510	372	<b>3</b> 59	346	327	324
	9	566	483	338	296	280	244	270
127-18	1	<b>484</b>	433	297	288	272	251	2 <b>43</b>
	9	502	413	255	213	192	176	192

CONFIDENTIAL

TABLE II. - Continued. COMBUSTION-CHAMBER WALL TEMPERATURES,  ${}^{\mathbf{O}}\mathbf{F}$ 

Series	Channel	Solid wal			Wire-clo	oth por	rous wal	L .
and run				T <sub>w,24</sub>	T. 72 C	T., 43	Tw,49.6	T., 57 5
							<del></del>	
127-19	1	454	401	264	249	232	219	207
	9	470	388	220	182	172	151	163
129-25	1	648	662	596	649	680	703	768
123-23	9	669	625	519	4/78	456	384	458
					2,0			
129-26	1	649	669	608	. 669	699	728	790
	9	672	632	540	499	488	397	476
	_	628	240	500	500	200		700
129-24	1 9	648	640	560	599	622 <b>4</b> 20	648 359	700
	9	040	600	481	433	420	339	429
129-23	1	618	630	552	581	611	642	686
	9	640	599	451	403	391	334	401
						·		
130-37	1	598	605	506	552	582	577	602
	9	605	577	467	425	396	359	419
130-32	,	640	CCE	CEO.	CO4	720	750	700
130-32	1 9	648 662	665 649	658 556	68 <b>4</b> 506	729 <b>4</b> 52	752 403	798 <b>4</b> 67
		002	043	330	300	402	-400	1 407
130-33	1	628	643	606	622	662	691	733
	9	640	622	498	448	408	368	428
							· ·	
130-31	1	622	632	586	608	631	638	665
	9	633	602	515	473	437	792	453
130-30	1	622	636	600	611	642	658	702
100-00	9	688	608	500	454	418	375	437
130-29	1	622	632	593	606	648	672	701
	9	638	608	492	448	410	370	430
170 74		004	607	000	252	007	077	
130-34	1  .9	664 ′ 674	681 682	692 538	751 478	823 427	877 378	890 <b>43</b> 2
· ·		074	002	336	470	461	376	436
130-35	1	676	695	718	806	891	930	948
	9	682	707	551	488	436	382	438
·								
130-36	1	. 685	703	735	845	930	955	978
	. 9	687	725	545	482	430	380	430
129-21	1	379	577	457	468	478	478	505
	9	592	541	390	351	348	<b>3</b> 98	<b>3</b> 56
[								
129-22	1	625	640	580	619	665	709	760
	9	653	650	417	362	352	299	355
129-20	1	630	633	E47	E74	617	CEO	707
163-60	1 9	620 650	631 629	541 397	57 <b>4</b> 3 <b>4</b> 7	617 339	652 290	707 340
	<u> </u>	.000	063	331	J#1		250	J*U

TABLE II. - Concluded. COMBUSTION-CHAMBER WALL TEMPERATURES, OF

Series and run	Channel	Solid wa			Wire-clo	oth po	rous wal	1
		Tw,10	Tw,19	Tw,24	Tw,32.6	Tw,41	<sup>T</sup> w,49.6	Tw,57.5
128-5	9	475 489	435 422	300 262	285 220	281 215	269 187	264 214
128-6	1 9	<b>4</b> 9 <b>3</b> 508	456 441	321 284	308 240	302 2 <b>3</b> 5	293 203	287 232
130-20	1 9	690 669	678 6 <b>4</b> 8	564 505	629 <b>4</b> 70	666 457	689 <b>4</b> 01	759 <b>4</b> 72
130-21	1	726	710	617	701	744	760	842
	9	721	676	588	572	527	<b>4</b> 90	558
130-18	1	652	6 <b>4</b> 9	537	569	603	629	703
	9	669	626	431	388	380	334	388
130-19	1	670	662	544	589	62 <u>7</u>	654	727
	9	682	6 <b>34</b>	465	<b>4</b> 22	415	364	<b>4</b> 28
129-19	1	650	672	589	647	692	718	830
	9	696	690	<b>425</b>	368	352	302	354
129-11	1	685	712	647	752	828	870	933
	9	7 <b>3</b> 2	7 <b>4</b> 8	492	<b>433</b>	<b>4</b> 18	354	412
129-10	1	662	689	600	680	738	713	857
	9	707	718	449	<b>3</b> 92	379	322	378
129-8	1	637	660	570	623	675	712	802
	9	678	677	408	353	<b>344</b>	297	340
129-9	1	6 <b>34</b>	652	546	589	628	650	727
	9	679	678	390	<b>33</b> 8	330	282	330
130-27	1	709 735	720 752	611 484	682 426	751 400	778 361	842 420
130-28-	——————————————————————————————————————	730 751	7 <b>4</b> 1	647 519	732 464	820 432	846 393	905 <b>449</b>
130-26	1 9	7 <b>4</b> 1 768	758 808	662 518	761 458	847 430	880 391	943 457
130-25	1	753	787	679	803	900	926	986
	9	787	813	532	472	948	408	478
130-22	1	723	741	530	577	602	616	680
	9	769	798	472	420	392	362	426
130-23	1	749	777	560	630	663	681	749
	9	690	8 <b>4</b> 5	522	478	447	<b>4</b> 16	490

TABLE III. - COOLING-AIR AND SHROUD TEMPERATURES, OF

Series	Channel			Cool	ing ai			Sì	Shroud wall				
and run	1	Ta,19 (a)	Ta,24	Ta,32.6	Ta,41	Ta,49.6	Ta,57.5	T <sub>s,24</sub>	Ts,41	T <sub>s,57.5</sub>			
127-27	1 .	112 121	214 186	20 <del>4</del> 179	195	185 167	178 165	169	188	194 			
127-26	1 9	107 117	200 175	182 11 <b>4</b>	184	175 157	166 15 <b>4</b>	160	175	179 			
127-25	1 9	101 108	170 152	157 108	157	150 1 <b>4</b> 0	145 135	138	147	150			
127-24	1 9	97 103	152 1 <b>4</b> 0	1 <b>43</b> 108	142	137 130	131 125	126	133	133			
127-23	1 9.	94 98	137 128	130 107	131	127 122	120 117	116	124	121			
127-28	1 9	94 98	136 128	130 123	130	127 122	123 118	116	125	123			
127-21	9	115 125	213 179	199 173	196	182 166	17 <b>4</b> 162	168	180	190			
127-20	1 9	105 117	190 160	178 101	175 	161 145	146 138	150	157	155			
130-17	1 9	104 113	171 153	162 151	159	153 140	132 132	139	144	141			
127-17	1 9	101 110	177 152	167 104	164 	153 138	138 132	140	148	147			
127-22	1 9	106 115	184 158	172 105	170	162 150	160 149	147	157	168			
130-24	1 9	107 117	175 159	166 154	165 	156 144	144 141	144 	151 	154 			
128-4	1 9	97 107	175 151	165 149	163	152 139	137 132	142	148	148			
129-18	1 9	101 112	170 151	161 155	160	133 135	148 126	138	144	138			
129-7	1 9	99 109	169 149	160 143	158	135 136	145 131	136	142	140			
129-32	1 9	104 115	171 154	164 155	163 	144 140	150 136	141	148 	146			
127-18	1 9	95 101	149 185	193 101	142	136 127	131 123	123	130	131 			

 $<sup>{}^{\</sup>mbox{\scriptsize a}}\mbox{\scriptsize Values}$  read from circumferential temperature profiles.

TABLE III. - Continued. COOLING-AIR AND SHROUD TEMPERATURES,  ${}^{\mathrm{O}}\mathrm{F}$ 

Series	Channel				ng air			Shroud wall				
and run	i.	Ta,19 (a)	<sup>Т</sup> а,24	Ta,32.6	Ta,41	Ta,49.6	Ta,57.5	T <sub>s,24</sub>	T <sub>s,41</sub>	T <sub>s,57.5</sub>		
127-19	1 9	92 97	137 127	133 122	131	127 120	121 115	115	121	120		
129-25	1 9	126 130	255 200	222 213	229 	242 181	224 186	195 	224 	257 		
129-26	1 9	129 134	26 <b>4</b> 207	228 219	236	254 185	232 192	200	232	273		
129-24	1 9	122 127	235 190	208 200	214	224 173	209 177	181	208	239		
129-23	1 9	117 122	223 182	200 207	205 	210 165	198 169	171	195	216		
130-37	1 9	112 120	219 190	193 181	198	195 163	204 171	167	191	209		
130-32	. 1 9	124 125	265 213	228 149	236	231 177	238 185	194	227	256 		
130-33	1 · 9	119 121	240 196	210 141	217	216 168	231 176	179	210	244		
130-31	1 9	117 122	241 201	209	215	210 171	214 ·180	180	206	226		
130-30	1 '	117 · 122	138 197	208 196	214	208 168	211 174	177	205	222		
130-29	1 9	115 121	235 194	207 131	213	210 166	217 171	176	206	230		
130-34	1 9	125 124	264 208	228 139	239	239 174	256 179	192	230	275		
130-35	1 9	127 -1-28-	273 _212_	235 137	248	249 177	176 183	196	239	198		
130-36	1 9	128 128 ·	27 <b>4</b> 210	236 140	250	256 177	290 183	198	246	315		
129-21	1 9	107 117	190 167	175 166	176	178 154	156 156	150	165	184		
129-22	1 9	116 121	219 _174	211 170	204	210 160	199 161	169	191	218		
129-20	1 9	114 119	210 170	193 165	197	203 156	192 157	164	183	205		

<sup>a</sup>Values read from circumferential temperature profiles.

TABLE III. - Concluded. COOLING-AIR AND SHROUD TEMPERATURES,  ${}^{\mathrm{O}}\!\mathrm{F}$  .

Series	Channel			Cooli	lng ai	r		Si	hroud v	vall
and run	:	Ta,19 (a)	<sup>Т</sup> а,24	Ta,32.6	Ta,41	Ta,49.6	Ta,57.5	T <sub>s,24</sub>	Ts,41	57.5, <sup>T</sup> s
128-5	1 9	89 96	140 131	135 130	134	130 122	121 117	117	125	123 
128-6	1 9	90 98	146 136	140 136	139	134 127	124 123	121	129	128
130-20	1 9	129 132	243 197	253 253	179 ·	22 <b>4</b> 179	239 190	191 	219	256 
130-21	1 9	137 142	273 218	248 334	259 	25 <b>4</b> 199	274 214	217	256	303 
130-18	· 1	117 122	215 177	199 170	203	194 158	186 156	169	186	199 
130-19	1 9	124 127	229	211 182	216	211 170	244 177	180	203	234
129-19	1 9	118 123	224 177	220 175	213	212 160	206 158	173	197	220
129-11	1 9	124 128	249 191	247 187	238	240 175	236 172	191	224	275 
129-10	1 9	118 125	233 182	214 197	220	228 164	<sup>-</sup> 21 <b>4</b> 155	179	204	238
129-8	1 9	114 119	217 171	200 170	205	191 15 <b>4</b>	1 <b>9</b> 5 150	166	186	199
129-9	1 -9	118 120	213 170	195 165	200	210 156	197 157	164	184	215
130-27	1 9	127 133	246 198	226 144	236	241 179	275 190	192	225	293
130-28	. 1 9	129 137	258 204	236 130	247	250 179	279 184	200	236	302
130-26	1. 9	129 137	260 205	239 197	251 	257 185	296 198	201	241	325
130-25	1 9	126 137	256 206	236 191	247 	245 180	255 186	199	235	283
130-22	1 9	127. 139	227 198	212 185	216	209 173	219 171	181	196	229
130-23	1 9	132 149	247 211	229 201	235	2 <b>33</b> 198	258 218	195	219	178

<sup>&</sup>lt;sup>a</sup>Values read from circumferential temperature profiles.

TABLE IV. - COMBUSTION-GAS AND COOLING-AIR PRESSURES

Series	Channel		Combu	stion-c	hamber st	atic p	ressures	, 1b/sq	in. abs		Cooling-air pressures, lb/sq in. abs								
and run		Pg,10	Pg,19	Pg,24	Pg,32.6	Pg,41	Pg,49.6	Pg,57.5	Pg,63.8	Pg,67.8	Pa,15	Pa,24	P <sub>B,24</sub>	Pa,32.6	Pa,41	Pa,49.6	Pa,57.5		
127-27	1 9	9.507	9.778	9.840	9.688	9.556	9.243	9.188	8.715	8.354	10.4	10.29 10.42	10.16 10.20	10.21 10.30	10.21 10.31	10.22 10.30	10.22		
127-26	1 9	9.493	9.757	9.813	9.660	9.521	9.194	9.132	8.625	8.326	10.62	10.49 10.66	10.29 10.37	10.37 10.51	10.38 10.52	10.39 10.51	10.38 10.50		
127-25	1 9	9.604	9.882	9.910	9.764	9.583	9.257	9.146	8.653	8.319	11.71	11.43 11.79	11.03	11.19 11.49	11.22 11.53	11.23 11.52	11.23 11.51		
127-24	1 9	9.701	9.979	9.993	9.833	9.625	9.285	9.139	8.646	8.319	13.05	12.49 13.11	11.86 12.33	12.14 12.65	12.19 12.71	12.20 12.70	12.21 12.69		
127-23	1 9	9.785	10.06	10.07	9.903	9.660	9.292	9.097	8.681	8.326	14.81	13.95 14.87	13.00 13.80	13.43 14.25	13.51 14.34	13.53 14.33	13.54 14.33		
127-28	1 9	9.785	10.06	10.08	9.903	9.646	9.299	9.104	8.646	8.340	14.70	13.84 14.75	12.88 13.67	13.31 14.13	13.39 14.22	13.42 14.22	13.42 14.21		
127-21	1 9	4.500	4.708	4.757	4.667	4.576	4.326	4.257	3,854	3.500	5.563	5.48 5.57	5.35 5.38	5.39 5.48	5.39 5.49	5.40 5.48	5.39 5.46		
127-20	1	4.542	4.750	4.778	4.694	4.590	4.340	4.250	3.833	3.479	6.055	5.912 6.077	5.700 5.790	5.780 5.928	5.790 5.939	5.795 5.93	5.790 5.918		
130-17	9	4.625	4.84	4.889	4.785	4.646	4.444	4.194	3.931	3.556	6.605	6.397 6.647	6.083 6.386	6.195 6.471	6.216 6.482	6.227 6.498	6.216 6.492		
127-17	1 9	4.569	4.778	4.819	4.715	4.597	4.354	4.250	3.875	3.500	6.493	6.301 6.536	6.025 6.163	6.121 6.322	6.142 6.344	6.153 6.33	6.147 6.323		
127-22	1 9	4.563	4.764	4.806	4.708	4.583	4.326	4.222	3.826	3.479	6.514	6.312	6.030 6.179	6.136 6.349	6.152 6.365	6.158 6.35	6.158 6.338		
130-24	9 .	4.569	4.785	4.826	4.736	4.590	4.389	4.146	3.854	3.465	6.470	6.281 6.509	5.973 6.260	6.079 6.345	6.100 6.355	6.105 6.366	6.100 6.366		
128-4	9	4.56	4.78	4.76	4.69	4.58	4.33	4.22	3.82	3.48	6.425	6.191 6.414	5.914 6.159	6.031 6.239	6.042 6.265	6.053	6.053 6.265		
129-18	9	4.576	4.792	4.813	4.750	4.611	4.431		3.910	3.514	6.61	6.39 6.65	6.08 6.40	6.21 6.47	6.22 6.48	6.23 6.48	6.23 6.49		
129-7	9	4.715	4.931	4.938	4.840	4.729	4.493	4.354	3.958	3.632	6.82	6.59 6.87	6.60	6.39 6.68	6.41	6.41 6.69	6.41 6.70		
129-32	9	4.625	4.833	4.854	4.785	4.646	4.465	6.438	3.922	3.611	6.748	6.499 6.791	6.175 6.515	6.313 6.600	6.329 6.610	6.334 6.175	6.334 6.621		
127-18	9	4.701	4.903	4.931	4.806	4.646	4.382	4.208	3.847	3.458	8.326	7.847 8.390	7.326 7.746	7.549 8.017	7.592 8.060	7.613 8.045	7.613 8.028		
127-19	9	4.806	5.000	5.000	4.889	4.701	4.417	4.208	3.847	.3,431	9.722	9.06	8.34 8.99	8.66 9.33	8.72 9.39	8.74 9.38	8.74 9.37		
129-25	1 9	14.63	14.55	14.39	13.93	13.25	12.65		10.38	8.382	15.81	15.43 15.88	15.02 15.47	15.17 15.58	15.20 15.60	15.23 15.60	15.23 15.61		
.129-26	1 9	14.58	14.51	14.36	13.90	13.23	12.63		10.36	8.431	15.59	15.25 15.66	14.87 15.28	15.02 15.38	15.04 15.39	15.06 15.40	15.06 15.41		
129-24	) 9	14.65	14760-	-14-42-	13.97	13.26_	12.65		10.38	8.375	16.23	15.52 16.37	14.81 15.61	15.08 15.82	15.14 15.86	15.16 15.87	15.18 15.89		
129-23	1 9	14.74	14.65	14.49	14.01	13.28	12.64		10.40	8.306	16.76	15.89 16.92	15.05 16.04	15.41 16.28	15.48 16.34	15.51 16.36	15.52 16.38		
130-37	1 9	16.04	16.00	15.97	15.47	14.49	13.73	12.76		8.374	17.46	17.00 17.54	16.48 17.03	16.67 17.18	16.72 17.21	16.74 17.24	16.74 17.24		
130-32	1 9	16.59	16.47	16.42	15.85	14.84	14.09	12.86	11.43	8.333	17.33	16.98 17.39	16.59 16.99	16.70 17.10	16.74 17.12	16.76 17.14	16.76 16.79		
130-33	1 9	16.69	16.55	16.49	15.91	14.88	14.12	12.90	11.50	8,409	18.01	17.53 18.08	17.01 17.56	17.19 17.71	17.23 17.74	17.26 17.77	17.25 17.77		

TABLE IV. - Concluded. COMBUSTION-GAS AND COOLING-AIR PRESSURES

Series	Channel		Combus	tion-cha	umber sta	atic pro	essures,	lb/sq ir	a. abs		_ ···	Coolin	g-air p	ressures	, 1b/sq	in. abs	
and run		Pg,10	p <sub>g,19</sub>	Pg,24	p <sub>g,32.6</sub>	Pg,41	Pg,49.6	Pg,57.5	Pg,63.8	Pg,67.8	Pa,15	Pa,24	Pa,24	Pa,32.6	Pa,41	Pa,49.6	pa,57.5
130-31	1 9	15.94	15.88	15.85	15.36	14.42	13.69	12.47	11.15	8.340	16.86	16.50	16.08	16.22	16.25	16.27	16.28
130-30	1 9	16.20	16.11	16.06	15.53	14.55	13.81	12.59	11.27	8.312	17.40	16.93 16.95 17.46	16.52 16.48 17.00	16.64 16.65 17.13	16.65 16.68 17.16	16.67 16.70 17.18	16.68 16.71 17.18
130-29	1 9	16.26	16.16	16.10	15.56	14.58	13.83	12.61	12.17	8.361	17.52	17.07 17.59	16.57 16.98	16.74 17.25	16.79 17.28	16.81 17.30	16.82 17.31
130-34	1 9	17.43	17.21	17.11	16.43	15.29	14.53	13.34	11.80	8.381	18.48	18.10 18.63	17.60 18.11	17.77 18.26	17.81 18.28	17.83 18.31	17.84 18.32
130-35	1 9	17.70	17.45	17.33	16.59	15.42	14.67	13.58	11.94	8.361	18.75	18.29 18.82	17.80 18.30	17.96 18.44	18.01 18.47	18.03 18.50	18.03 18.50
130-36	1 9	17.94	17.67	17.53	16.76	15.53	14.83	13.81	12.10	8.381	19.18	18.70 19.25	18.16 18.70	18.35 18.85	18.39 18.88	18.41 18.91	18.41 18.91
129-21	1 9	11.87	11.88	11.77	11.43	10.90	10.36		8.576	7.153	14.42	13.64 14.67	12.75 13.79	13.15 14.06	13.22 14.11	13.25 14.13	13.26 14.15
129-22	1 9	13.35	13.20	13.00	12.48	11.78	11.21		9.153	7.056	16.42	15.33 16.60	14.26 15.51	14.72 15.83	14.80 15.89	14.85 15.92	14.87 15.94
129-20	9	11.18	11.06	10.90	10.45	9.868	9.368		7.604	5.840	14.54	13.84 14.65	13.14 13.96	13.45 14.16	13.50 14.21	13.52 14.22	13.53 14.23
128-5	1 9	6.72	6.80	6.72	6.54	6.22	5.78	5.44	4.74	3.60	11.33	10.52 11.32	9.70 10.56	10.08 10.82	10.14 10.90	10.17 10.91	10.17
128-6	9	6.67	6.74	6.65	6.47	6.17	5.74	5,40	4.71	3.51	10.67	9.95 10.66	9.24 9.98	10.17	9.62	9.64 10.29	9.64 10.30
130-20	9	8.174	8.132	8.076	7.778	7.382	6.993	6.354	5.590	3.500	9.854	9.321 9.619	9.013 9.342	9.119 9.417	9.140 9.433	9.151 9.449	9.151 9.496
130-21	9	8.056	8.021	7.972 8.319	7.681	7.319	6.958	6.292	5.549	3.528	8.798	8.650 8.826	8.464 8.661	8.523	8.533 8.703	8.544 8.714	8.544
130-18	1 9 1	8.451	8.396	8.236	7.986	7.549	7.146	6.472	5.715	3.535 3.528	10.75	10.36 10.82 9.896		10.05 10.52 9.641	10.08 10.55 9.662	10.10 10.57 9.678	10.10 10.57 9.678
129-19	9	9.049	8.931	8.764	8.382	7.910	7.528	0.431	6.014	3.646	12.15	10.28		10.02	10.04	10.07	10.07
129-11	9	8.951	8.840	8.681	8.299	7.854	7.514		6.007	3.542	10.98			11.71	11.74		11.77
129-10	9	8.972	8.854	8.694	8.299	7.861	7.514	6.875	6.000	3.563	11.50		10.66		10.79		10.80
129-8	9	9.090	8.979	8.806	8.396	7.958	7.583	6.924	6.056	3.438	12.08	11.57	11.11	11.23	11.27	11.27	11.28
125-9	9	9.097	8.986	8.806	8.396	7.944	7.556	6.903	6.083	3.590	12.70	12.22	11.65	11.70	11.84		11.87
130-27	9	9.153	9.042	8.944	8.542	7.986	7.576	6.896	6.083	3.500	11.51	11.11	10.64	10.82	12.40	10.86	12.42
130-28	9	9.132	9.000	8.917	8.528	7.965	7.569	6.944	6.090	3.500	11.04		10.33		10.49	10.51	11.30
130-26	9 1 9	9.361	9.229	9.118	9.319	8.118	7.729	7.090	6.250	3.500	11.61	11.20	10.36	10.96	10.85 10.98 11.38	11.00	10.86
130-25	1 9	9.549	9.389	9.264	8.792	8.264	7.868	7.118	6.313	3.528	11.87	11.46	11.05	11.21	11.38 11.24 11.64	11.25	11.40 11.26 11.66
130-22	1 9	5.750	5.681	5.611	5.340	5.028	4.757	4.340	3.799	2.208	8.430	8.107 8.474	7.687 8.128	7.841 8.229	7.868 8.250	7.879 8.261	7.879 8.266
130-23	1 9	5.604	5.542	5.472	5.208	4.903	4.660	4.250	3.722	2.229	7.048	7.483	7.175 7.515	7.291 7.589	7.307	7.323 7.610	7.323 7.610

TABLE V. - AIR-FLOW CALIBRATION DATA OF AFTERBURNER AT AMBIENT TEMPERATURE

	Pa,57.5	14.34	14.33	14.62	14.81	15.05	15.49	15.90	14.99	16.94	17.37	17.87	18.37	18.85	8.852	9.286	10.34	10.95	11.83	12.62	3.436	5.066
in aba	4	14.35	14.35	14.63	14.82	15.06	15.49	15.90	14.98	16.94	17.36	17.86	18.37	18.83	8.857	9.292	10.34	10.95	11.63	12.62 12.81	3.319	4.843
115/80	Pa,41	14.35	14.34	14.62	14.81	15.05	15.47	15.88	14.96	16.92	17.34	17.84	19.52	18.81	8.852	9.286	10.33	10.94	11.82	12.60	3.319	4.832 5.087
nregaures	Pa,32.6	14.34	14.33	14.60	14.78	15.00	15.41	15.81 16.31	14.85	16.80	17.22 18.15	17.70 18.75	18.18	19.63	8.842 8.964	9.260	10.27	10.86	11.70	12.46	3.308	4.811 5.061
		14.31	14.31	14.54	14.70	14.88	15.23	15.56	14.52	16.38	16.73	17.16	17.58	17.96	8.778	9.143	9.990	10.52	11.26	11.95	3.234	4.672
Cooling-air	Pa,24	14.39	14.39	14.73	14.98	15.28	15.83	16.32	15.48	17.39	17.85	18.40	18.94	19.47	9.086	9.451	10.67	11.34	12.31 13.26	13.19	3.415	5.013
	Pa,15	14.42	14.42	14.82	15.11	15.45	16.08	16.67	17.46	18.11	18.70	19.36	20.02	20.68	9.05	9.63	11.15	11.83	13.03	14.15	3.52	5.212
Channel		16	- 6	6	- 6	46	4.6	<b>д</b> б	۰.6	1 6	1 6	7 6	٦6	- 6	<b>~</b> 6	1 6	ч 6	ч 6	1 6	H 6	٦6	1 6
	Pg,67.8	14.08	14.08	14.08	14.08	14.08	14.08	14.11	14.06	14.08	14.08	14.08	14.08	14.08	8.340	8.361	8.264	8.361	8.361	8.340	3.493	3.479
aha.	63.8	14.08	14.11	14.08	14.08	14.08	14.08	14.10	14.08	14.08	14.08	14.11	14.10	14.08	8.389	8.410	8.264	8.375	8.424	8.347	3.472	3.479
Th/so in.	7.5	14.10	14.10	14.10	14.08	14.09	14.08	14.11	14.07	14.06	14.06	14.08	14.10	14.09	8.278	8.361	8.229	8.354	8.368	8.336		3.465
Dressures.	Pg,49.6 P	14.10	01.	14.10	14.08	60.	8	11.	20	8	14.08	66.	ti.	.10	8.285	8.361	8.243	8.361	8.375	8.333	<del>'</del> -	3.472
		9.	14.10 14	14.10 14	14.08	14.09 14	4.08	4.11	4.07 14.	4.08	14.08	1.10	4.12 14	4.10 14	9.282	8.361	8.243	8.361	8.375 8	8.333	<u> </u>	3.472
her static	φ	10 14	14.10	14.10	14.10	60,	90,	41 11.	.07	99.	14.08	14.10   14	.12	14.10 14	8,285	8.361	8,236	8.361	8.375	8,333		3.472
red o	Pg,24 Pg	14.10 14	.10	01.	8.	14	08	11.1	14	90.1	8	.10	.12	10	8.285 8	8.361 8	8.243 8	8.361 8	8,375 8	8.340 8	-	3.472 3
Combiset fon-chamber	P8,19 P	.10	1.10	1.10	1.09	1.09	1.08	11.11	1.07	14	1.08	1.10	1.12	1.10	8.285	8.368	8.250 8	8.368	8.389	8.340 8	-	3.472 3
	Pg, 10 P	14.10 14	14.10 14	14.10 14	14.09 14	14.09 14	14.08 14	14.11 14	14.07	14.08 14	14.08 14	14.10 14	14.13 14	14.10 14	8.285	8.368	8.250	8.368	8.389	8.340		3.472
Cool tag-		534 1	527	530	531	532	534	535	534	535	534	535	535	535 1.	533	232	225	232	232	532	532	225
Managarad		0.9695	1.005	1.596	1.955	2.296	.850	3.310	3.914	4.315	4.678	.083	5.441	5.810	1.255	01.1	2.799	3,20	3.805	4.344	.9033	1.313
Man	Ø	o		1.	Ä	8		ю.	8		- <del>-</del> -		φ,	5.6				ю —	ъ.	·;	<del>-</del> ,	
Ambient	tank pres- sure, 1b/sq ft ab	2028	2028	2028	2028	2028	2028	2028	2028	2028	2028	2028	8202	2028	1195	1195	1192	1196	1200	1192	497	493
Series	<u>c</u>	127-14	127-2	127-3	127-4	127-5	127-6	127-7	127-8	127-9	127-10	11-721	127-12	127-13	127-35	127-36	127-37	127-38	127-39	127-40	127-34	127-33
_																						

TABLE V. - Continued. AIR-FLOW CALIBRATION DATA OF AFTERBURNER AT AMBIENT TEMPERATURE

	Pa,57.5	5.968	5.826	6.825	7.793 8.570	9.495	9.860	10.40	10.92	11.92	12.56	9.350	9.820	10.38	11.06	11.82	4.630	5.353	6.275	7.236	8.130
pressures, 1b/sq in. abs	Pa,49.6	5.968	5.826	6.825	7.793	9.500	9.860	10.39	10.92	11.92	12.55	9.365	9.815	10.38	11.055	11.82	4.630	5.353	6.275	7.236	8.125
	Pa,41	5.963	5.816	6.814	7.782	9.495	9.850	10.38	10.91	11.90	12.53 13.78	9.350	9.800	10.365	11.014	11.805	4.608	5.340	6.268	7.220	8.118
	Pa,32.6	5.905	5.768	6.740	7.687	9.470	9.800	10.32	10.84	11.68	12.38	9.335	9.760	10.31	10.95	11.70	4.605	5.305	6.22	7.150	8.020
Cooling-air p	Pa,24	5.702	5 5.571	7 6.474	7.357	9.340	9.620	10.005	5 10.52	11.36	11.95	9.190	9.560	10.04	10.60	11.26	4.491	5.122	5.958	7.691	7.680
Coolir	P. 24	6.282	3 6.135 - 6.592	7.197	8.25 - 9.038	9.630	- 10.06	10.65	11.245	12.38	- 14.48	9.490	10.02	10.63	11.40	12.26	4.985	5.938	3 6.575 - 7.118	8 7.610	3 8.945
-	Pa,15	6.660	6.483	7.705	8.91	9.847	10.40	11.11	11.82	13.20	14.11	9.722	10.38	11.13	12.04	13.10	4.930	5.770	6.993	8.138	9.263
Channel		1 6	- G -	. 16	16	<b>д</b> 6	<u>ч</u> ю́	ر م م	1 6	16	<b>д</b> 6	H 6	7 6	7 6	.1 6	. ~ 6	1.6	7.6	16	16	1
	Pg,67.8	3.479	3.431	3.528	3.451	8.542	8.389	8.458	8.534	8.389	8.340	8.368	8.326	8.444	8.375	8.333	3,493	3.417	-	-	-
lb/sq in. abs	Pg,63.8	3,486	3.438	3.486	3.465	8.556	8.410	8.493	8.549	8.403	9.385	-	8.326	8.465	8.403	8.375	3.493	-	3.465	3.535	3,500
	Pg,57.5	3,486	3,431	3.514	3.444	;											3.479	3,438	3,451	3.493	3.486
pressures	Pg,49.6	3.486	.3,438	3.528	3.465	9.542	8.424	8.486	8.542	8.396	8.340	8.368	8,333	8.444	8.410	8.333	3,486	3,438	3.458	3.493	3.493
static pr	Pg,41	3.486	3.444	3.528	3.465	8.542	8.424	8.493	8.549	8.403	8.340	8.368	8.333	8.444	0.410	6.333	3.486	3.438	3.458	3.507	3.500
	Pg,32.6	3.486	3.444	3.528	3.465	8.542	8.424	8.493	8.549	8.403	8.340	8.368	8.333	8.444	8.410	8.333	3.486	3.438	3,465	3.507	3.507
Combustion-chamber	Pg,24	3.486	3.444	3.528	3.465	8.542	8.431	8.493	8.549	8.403	8.340	8.368	8.333	8.444	8.417	8.333	3.486	3.438	3.465	3.507	3.507
Combus	pg,19	3.493	3.444	3.528	3.465	9.556	8.438	8.500	9.556	8.403	8.347	8.375	8.340	8.444	8.417	8.347	3.486	3.451	3.465	3.507	3.507
	Pg,10	3.493	3.444	3.528	.3.465	8.549	8.438	8.500	8.549	8.403	8.347	8.375	8.340	8.444	8.417	8.347	3.486	3.451	3.465	3.507	3.507
	air tem- pera- ture, OR	533	533	533	533	534	534	534	534	534	534	538	537	53.1	537	538	528	529	530	230	531
Measured	cooling- air flow, lb/sec	1.822	1.895	2.380	2.849	1.733	2.202	2.633	3.011	3,783	4.230	1.757	2.241	2.657	3.194	3.751	1.126	1.554	2.023	2.459	2,882
Ambient	tank pres- sure, lb/sq ft abs	495	491	498	. 264	1230	1208	1218	1229	1208	1201	1205	1199	1216	1206	1200	503	492	495	205	205
Series	and run	127-32	127-29	127-31	127-30	129-12	129-13	129-14	129-15	129-16	129-17	129-27	129-28	129-29	129-30	129-31	129-2	129-3	129-4	129-5	129-6

TABLE V. | Concluded. AIR-FLOW CALIBRATION DATA OF AFTERBURNER AT AMBIENT TEMPERATURE

Г	in						0::2						·^ ·	m 10		10.~	01.01			·o ~		
	Pa,57.5	14.99	16.71	17.09	8.505	8.788	9.240	9.729	10.21	10.94 11.81	11.62	12.10	4.066	4.708	5.724	6.615	7.782	3.069	3.909	4.576 5.028	5.797	6.379
	Pa,49.6	14.99	16.71	17.09	8.505	8.904	9.245	9.729	10.28	10.94	11.62	12.09	3,763	4.995	5.724	6.615	7.777	3.079	3.909	5.033	5.797	6.379
TONE		14.99		17.06	8.505	8.899	9.240	9.724	10.90	10.01	12.64	13.26	3.758	4.702	5.718	6.604	7.681	3.069	3.904	5.012	5.786	6.368
TWOTHWE JUNET	Ps,24 Ps,24 Ps,32.6 Ps,41	14.97		16.94	8.505	8.894	9.218	9.682	10.21	10.84	12.56	13.18	3.758	4.681	5.676	6.541	7.761.	3.058	3.883	4.534	5.733	6.299
1	Pa,24 P.	14.90 14		16.61	8.494 8	8.734 8.851	9.112	9.522	10.01	10.57	11.16 11	11.57	4.013	4.580	5.511	6.312	8.372	3.026	3.771	4.385	5.521	6.060
AMDIENT	Pa,24 Pa	15.08 14		17.47 16	8.515 8	8.935 8	9.346 9	9.889 9	10.53 10	01 72.11	12.01	12.54 11 12.76 12	3.822 4	5.133 4	5.963 5	6.934 6	9.105	3.015 3	4.069 3	5.224 4	6.094 5	6.708 6
AL AM	Pa, 15 Pa	15.24 15	17.81	18.34 17	8.541 8	8.930 8	9.569	10.25 9	11.08 10	12.01	16	13.57 12	4.215 3	5.069 4	6.340 5	7,465 6	8.881 8	3.111 3	4.312 4	5.118 4	6.583 6	7.270 6
	<del>,</del>	1 15	17 17 9	1 18	в ; 	9 ;	6 ;	0 1	11 6	1 12	1 6	13	4 ;	. 1 6	9 ;	7 -	8 ;	91	4 :	2 ;	9 ;	1 2
	8.																					
WEINDOWN TOWN	Pg,67.8	14.39	14.39	14.39	8.347	8.326	8.347	8.368	8.347	8.319	8.388	8.319	3,535	3.500	3.618	3.563	2.569	2.201	2.188	2.208	2.236	2.243
	P. 63.8	14.42	14,39	14.41	8.354	8.347	8.395	8.395	8.423	8.347	8.409	8.388	3.514	3.542	3.604	3,563	3,597	2.208	2.188	2.181	2.229	2.271
יייין א	* <del></del>	14.39	14.39	14.42	8.347	:	-	!	i				3.500	3,486	3.618	3.563	3.604	2.194	2.208	2.208	2.250	2.271
5	Pg,49.6	.39	39	40	8.333	8.347	8.374	8.409	8.388	8.361	8.430	8.347	3.500	3.479	3.604	3.556	290	2.194	2.188	2.188	2.22	2.243
NOT THIS TOTAL	8,19 Pg,24 Pg,32.6 Pg,41 Pg,49.6 Pg,57.5	14,39 14	14.39 14	14.40 14	8.333 8	8.347 8	8.374 8	8.409 8	381	8.340 8	8.416 8	8.333 8	200	3.479 3	3.604	3.556 3	3.590 3.	2.194 2	2.188 2	2.188 2	2.222 2	243
	Pg,32.6 Pg	1		.41 14	8.333 8	8.340 8	8.368 8	8.416 8	8.388 8.		8.437 8		.500 3.	3.479 3	3.611 3	3.556 3	390	2.194 2		2.188 2	2.229	.243 2.
# OT 1-1114	-cnamo	.39 14.39	.39 14.39	.40 14.4			368		.381 8.3	54 8.361		47 8.361	.500				590 3.5		94 2.201			0
	Pg,24	17.	7.		60 8.333	9.347	-0	00	8	8.354	87 8.430	8.347	٠	3.479	11 3.604	3.556	.604	2.194	1 2.194	84 2.188	627.2 62	2.250
• 1	17	14.40	14,39	14.41	9 8.340	8.354	8.381	8 8.416	6.395	1 8.361	7 8.437	8.361	3.500	9 3.479.	1 3.611	3 3.563	<u>ب</u>	2.194	1 2.201	2.194	9 2.229	7 2.257
Daniel and	pg,10	14.40	14.39	14.42	8.340	8.354	8.381	8.416	8.395	8.361	8.437	8.354	3.500	3.479	3.611	3.563	3,604	2.194	2.201	2.194	2.229	2.257
	air tem- pera- ture,	533	223	533	536.	536	536	536	536	;	536	;	529	530	530	532	532	532	;	.)	}	533
-	cooling- air flow,	1.84	3.95	4.34	42:	1.06	1.23	2.14	2.69	-	3.67	- <u>i</u>	2.	1.22	1.76	2.23	2.76	.88	_ _	-		2.22
i	tank pres- sure,	2072	2012	2072	1202	1199	1202	1205	1202	1198	1208	1198	509	504	521	513	514	317	315	318	322	323
-	end run t	130-5	130-3	130-4	130-38	130-39	130-40	130-41	130-42	130-43	130-44	130-45	130-7	130-8	130-,9	130-10	130-11	130-12	130-13	130-14	130-15	130-16

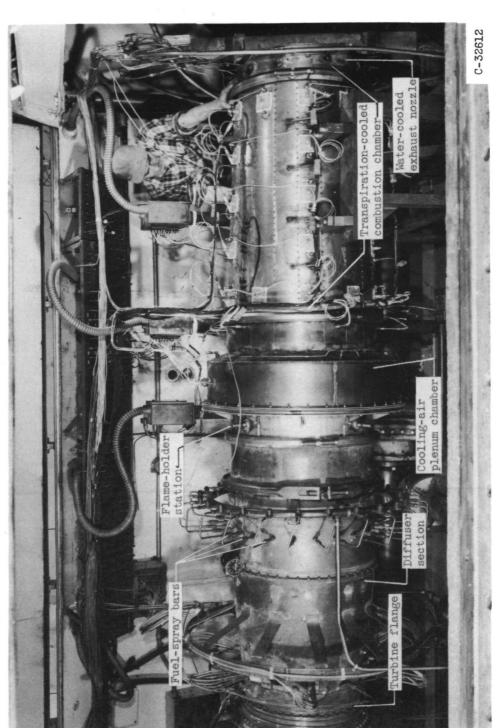
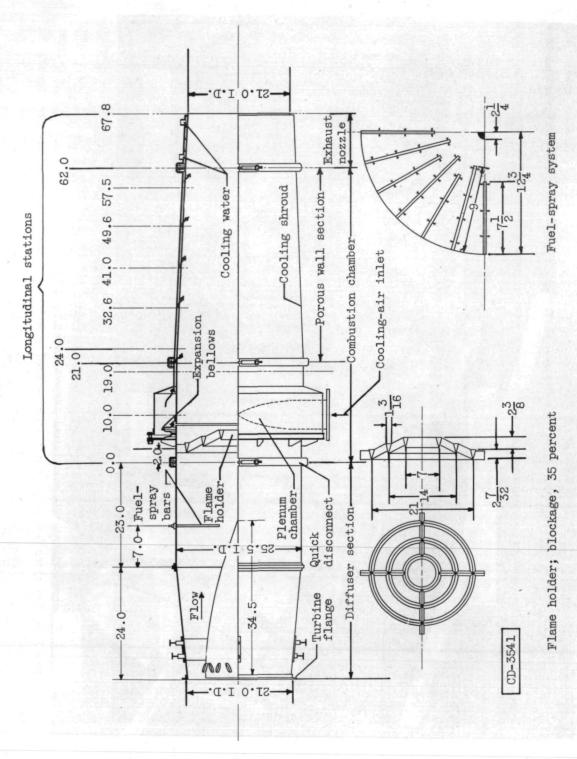


Figure 1. - Afterburner installation in altitude test chamber.



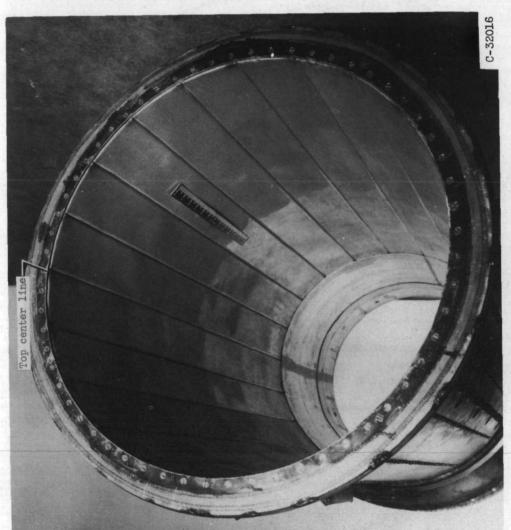


(All dimensions in inches.) Sectional view of afterburner. 3 Figure

NACA RM E54E25



Figure 3. - Wire-cloth porous combustion-chamber wall before assembly of structural cooling shroud.



(a) Before cooling investigation.

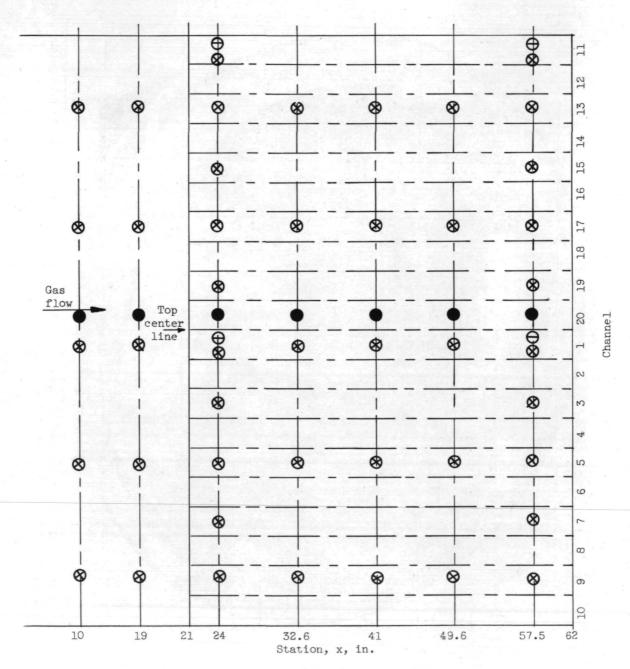
Figure 4. - Interior view of experimental transpiration-cooled afterburner with porous combustion-chamber wall fabricated from brazed and rolled wire cloth. Exhaust nozzle removed.



(b) After 4 hours 10 minutes of afterburning.

Figure 4. - Concluded. Interior view of experimental transpiration-cooled afterburner with porous combustionchamber wall fabricated from brazed and rolled wire cloth. Exhaust nozzle removed.

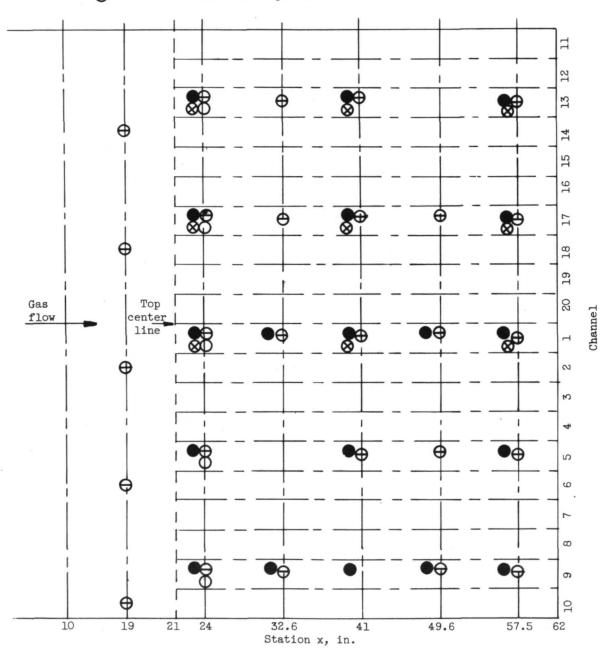
- Combustion-gas static pressure
- Wire-cloth or solid metal wall air-side temperature
- O Wire-cloth gas-side temperature



(a) Wire-cloth and combustion-gas instrumentation.

Figure 5. - Schematic development showing locations of temperature and pressure instrumentation on wire-cloth porous-wall afterburner.

- Cooling-air static pressure
- O Cooling-air total pressure
- Occiling-air temperature
- ⊗ Shroud outside-skin temperature



(b) Shroud and cooling-air instrumentation.

Figure 5. - Concluded. Schematic development showing locations of temperature and pressure instrumentation on wire-cloth porous-wall afterburner.

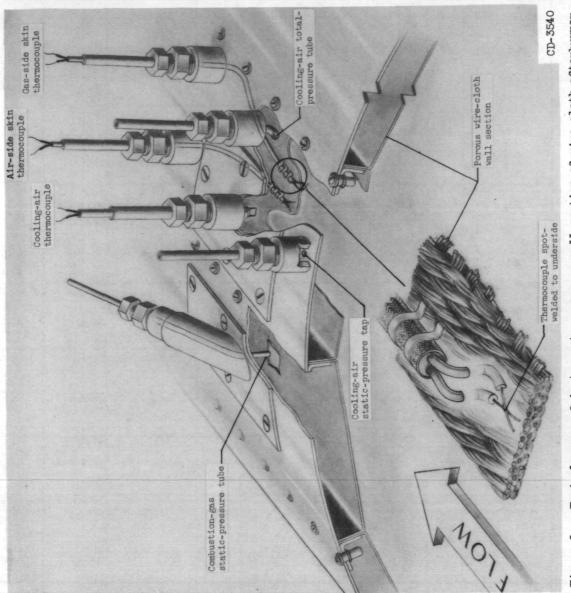
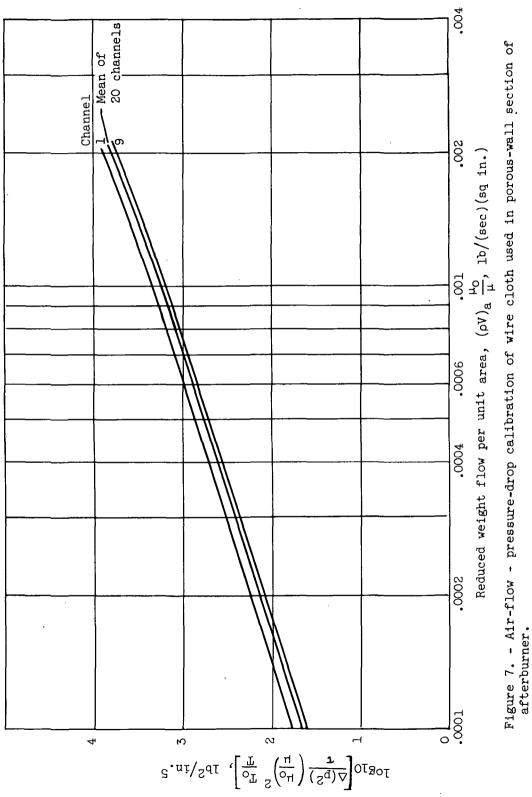
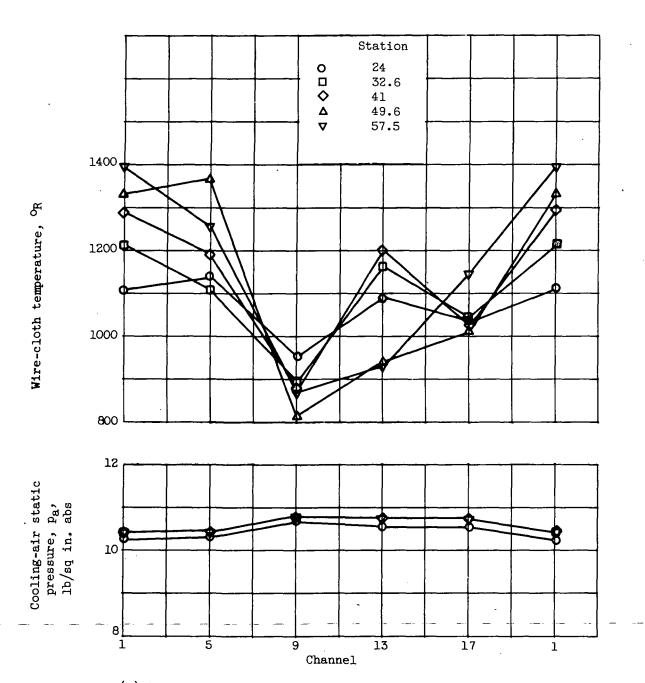


Figure 6. - Typical group of instruments on porous-wall section of wire-cloth afterburner.

3295

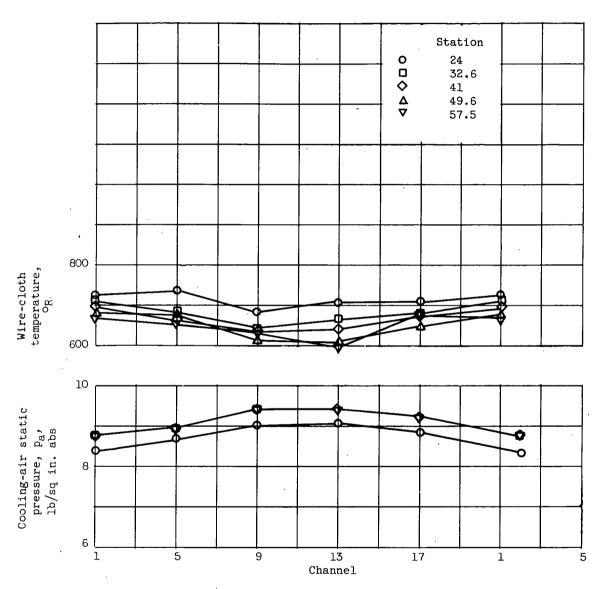


Pressure-drop parameter,



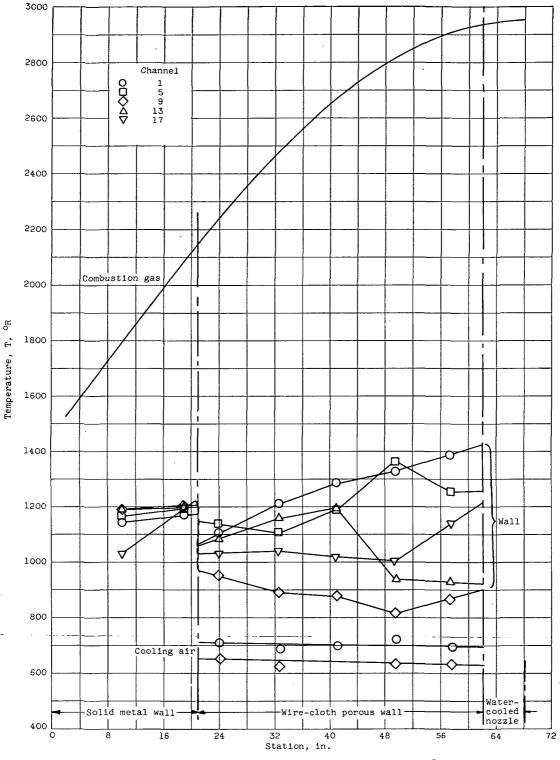
(a) Afterburning. Exhaust-gas temperature, 2954° R; total flow ratio, 0.0716.

Figure 8. - Typical circumferential profiles of wire-cloth temperature and cooling-air static pressure. Altitude, 35,000 feet; flight Mach number, 1.0.



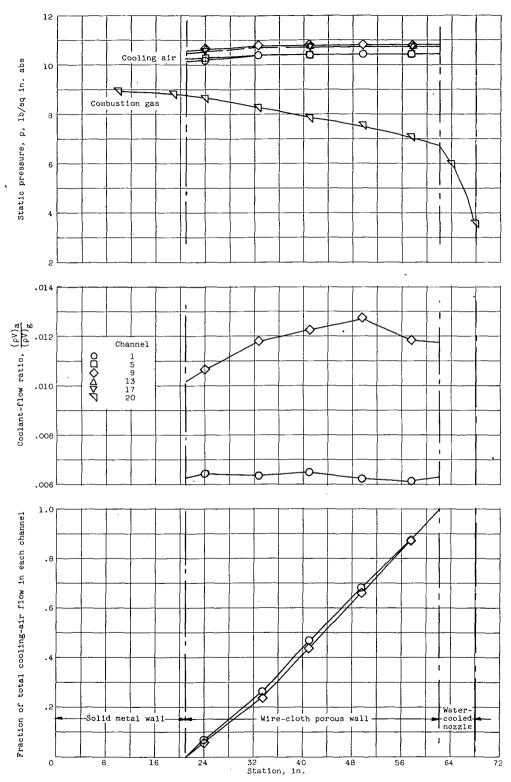
(b) Nonafterburning. Exhaust-gas temperature,  $1249^{\circ}$  R; total flow ratio, 0.0951.

Figure 8. - Concluded. Typical circumferential profiles of wire-cloth temperature and cooling-air static pressure. Altitude, 35,000 feet; flight Mach number, 1.0.



(a) Afterburning temperature profiles. Exhaust-gas temperature,  $2954^{\circ}$  R; total flow ratio, 0.0716.

Figure 9. - Typical longitudinal profiles for wire-cloth afterburner. Altitude, 35,000 feet; flight Mach number, 1.0.



(b) Afterburning static-pressure and coolant-flow profiles. Exhaust-gas temperature,  $2954^{\rm O}$  R; total flow ratio, 0.0716.

Figure 9. - Continued. Typical longitudinal profiles for wire-cloth afterburner. Altitude, 35,000 feet; flight Mach number, 1.0.



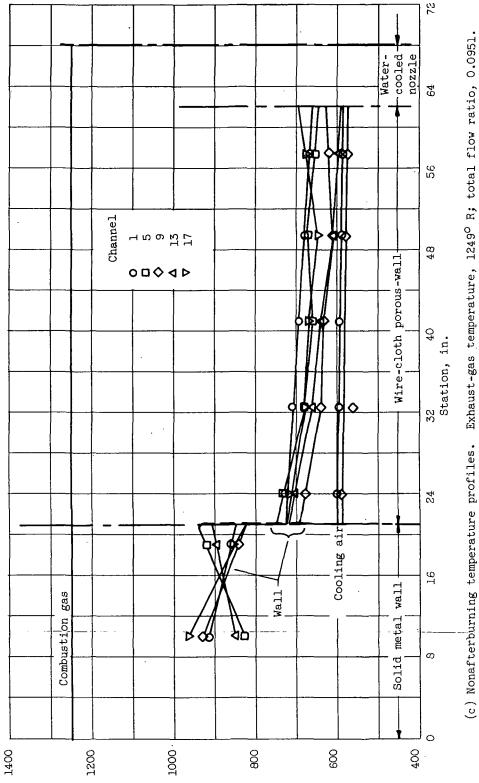
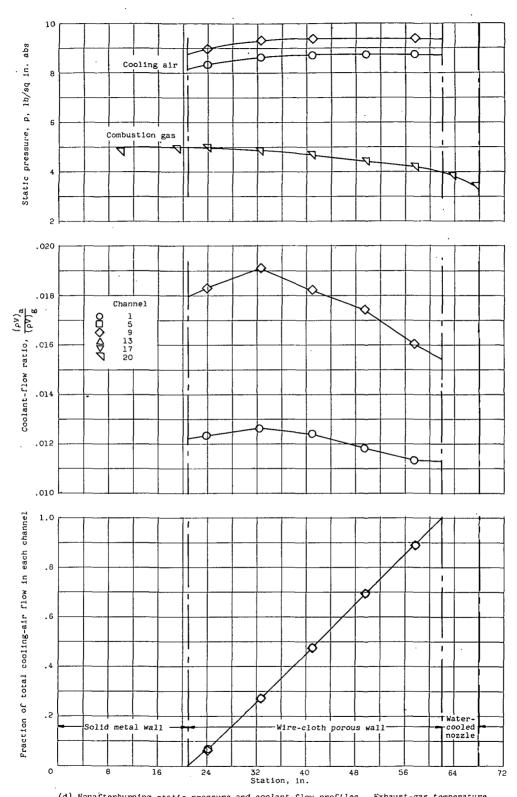


Figure 9. - Continued. Typical longitudinal profiles for wire-cloth afterburner. Altitude, 35,000 feet; flight Mach number, 1.0.

Hemperature, T. Temperature



(d) Nonafterburning static-pressure and coolant-flow profiles. Exhaust-gas temperature,  $1249^{\circ}$  R; total flow ratio, 0.0951.

Figure 9. - Concluded. Typical longitudinal profiles for wire-cloth afterburner. Altitude,  $\cdot$  35,000 feet; flight Mach number, 1.0.



Figure 10. - Appearance of greasy smudge on wire cloth after 4 hours 10 minutes of afterburning.

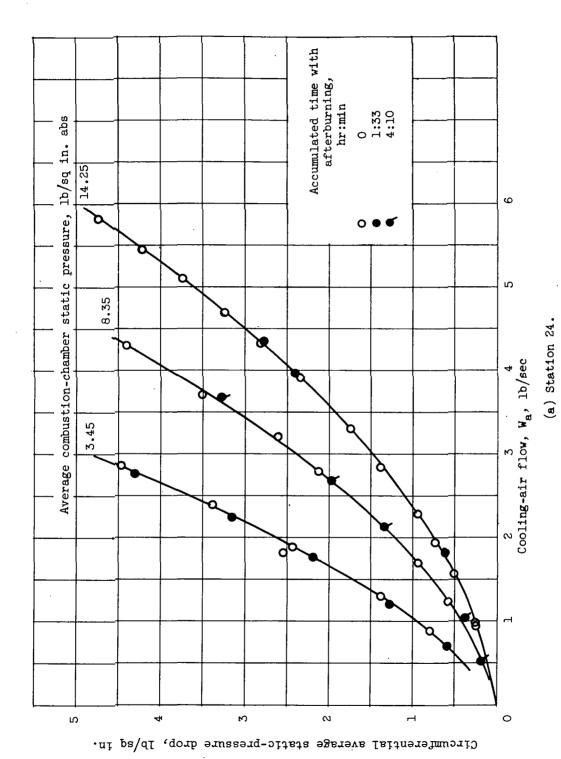
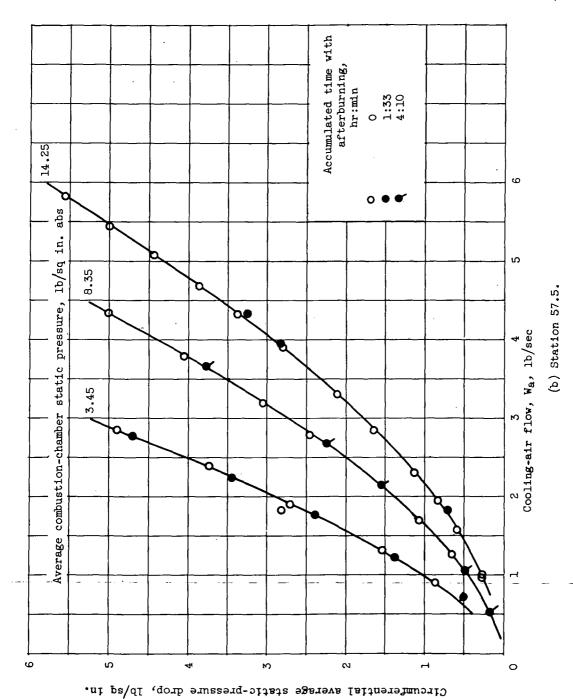
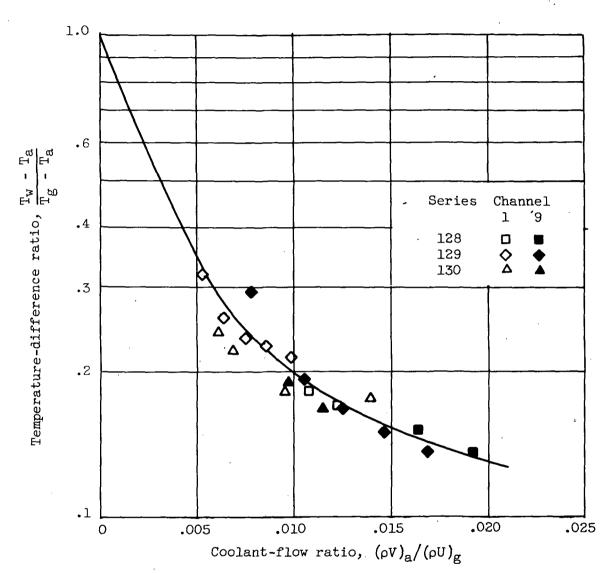


Figure 11. - Variation of circumferential average pressure drop across wire cloth with total measured cooling-air flow.

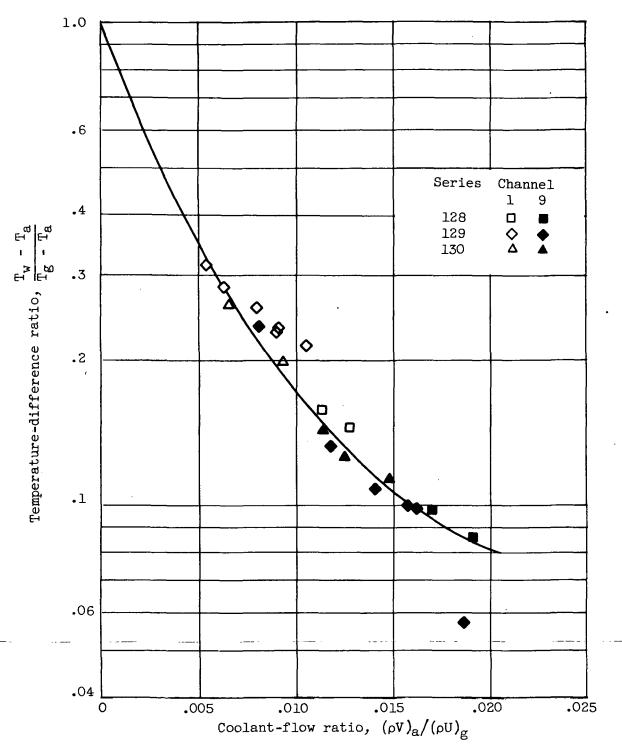


- Concluded. Variation of circumferential average pressure drop across wire cloth Figure 11. L



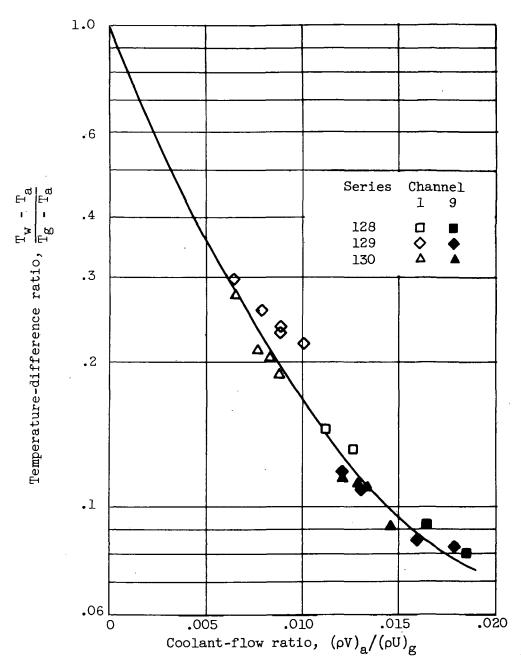
(a) Reynolds number, approximately 75,000.

Figure 12. - Correlation of afterburning cooling data for wire-cloth afterburner.



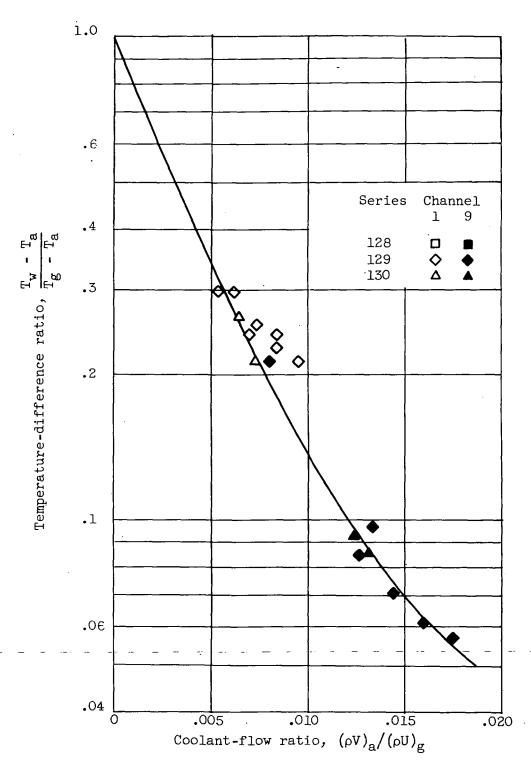
(b) Reynolds number, approximately 300,000.

Figure 12. - Continued. Correlation of afterburning cooling data for wire-cloth afterburner.



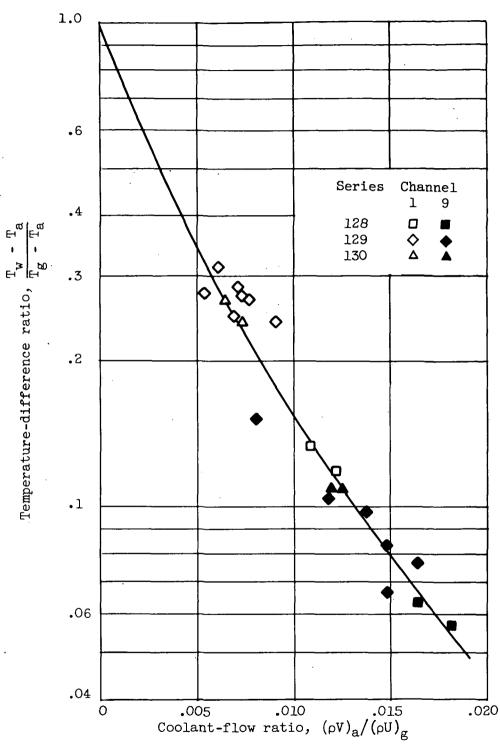
(c) Reynolds number, approximately 500,000.

Figure 12. - Continued. Correlation of afterburning cooling data for wire-cloth afterburner.



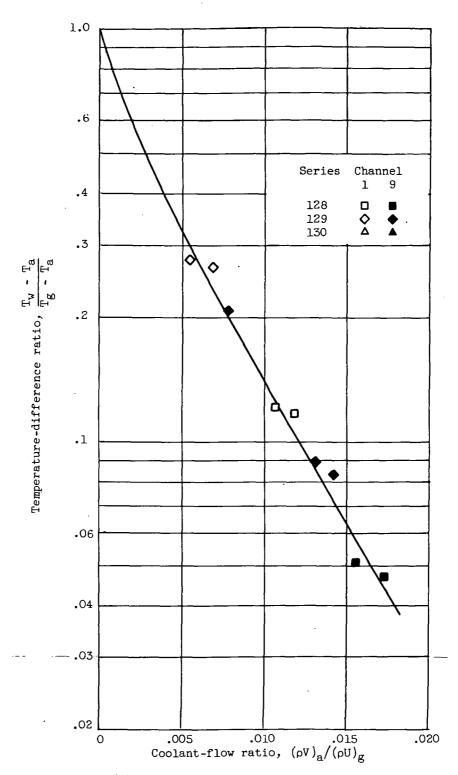
(d) Reynolds number, approximately 800,000.

Figure 12. - Continued. Correlation of afterburning cooling data for wire-cloth afterburner.



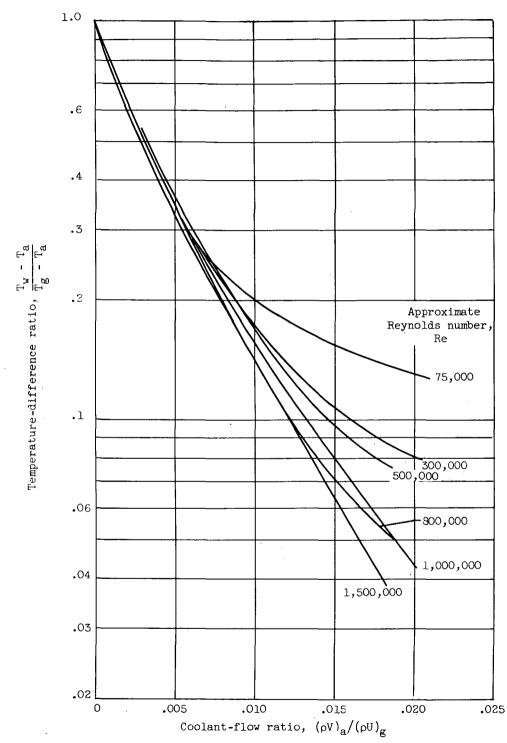
(e) Reynolds number, approximately 1,000,000.

Figure 12. - Continued. Correlation of afterburning cooling data for wire-cloth afterburner.



(f) Reynolds number, approximately 1,500,000.

Figure 12. - Continued. Correlation of afterburning cooling data for wire-cloth afterburner.



(g) Mean curves for approximate Reynolds numbers of 75,000 to 1,500,000.

Figure 12. - Concluded. Correlation of afterburning cooling data for wire-cloth afterburner.

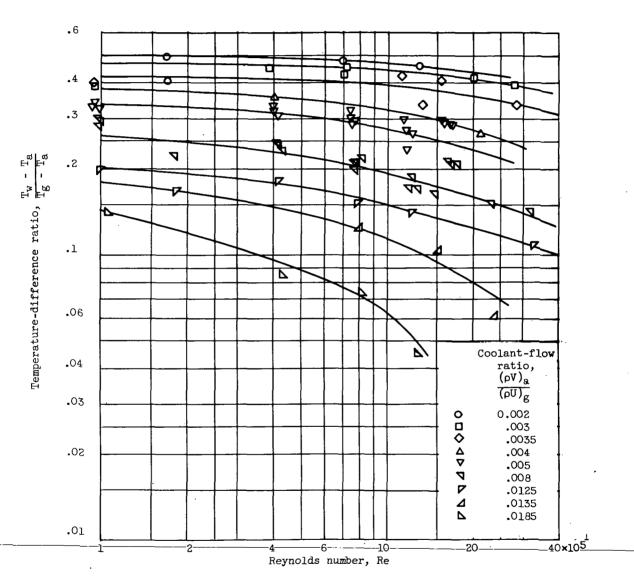


Figure 13. - Variation of temperature-difference ratio with Reynolds number for nonafterburning cooling data.

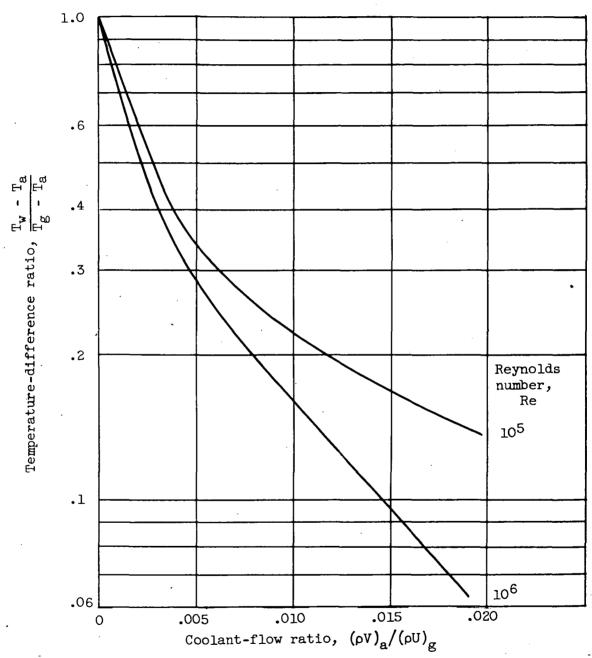


Figure 14. - Correlation of nonafterburning cooling data for wire-cloth afterburner.

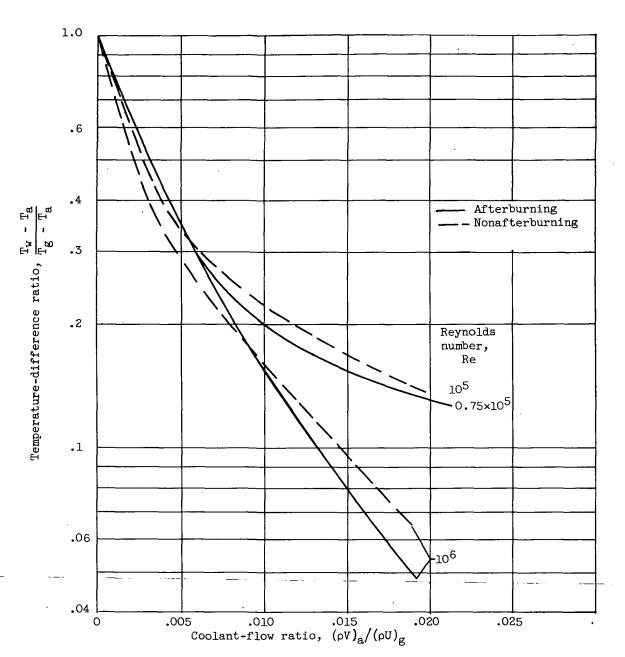


Figure 15. - Comparison of cooling correlations for afterburning and nonafterburning for wire-cloth afterburner.

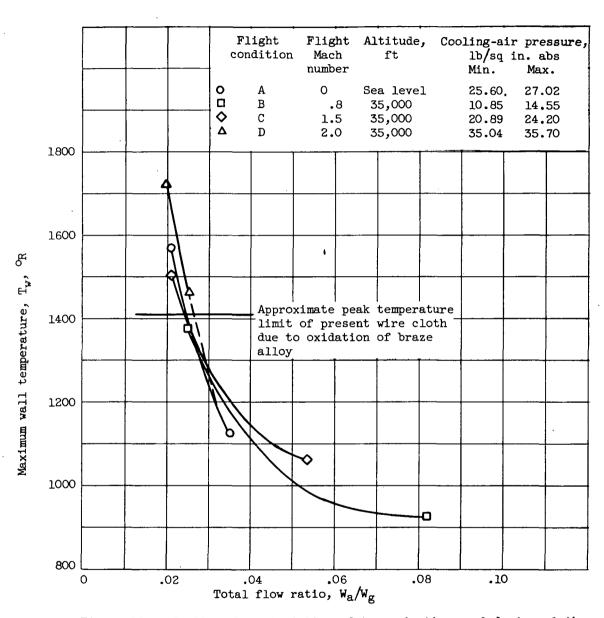


Figure 16. - Cooling characteristics of transpiration-cooled wire-cloth afterburner having uniform permeability distribution. Exhaust-gas temperature,  $3700^{\circ}$  R.

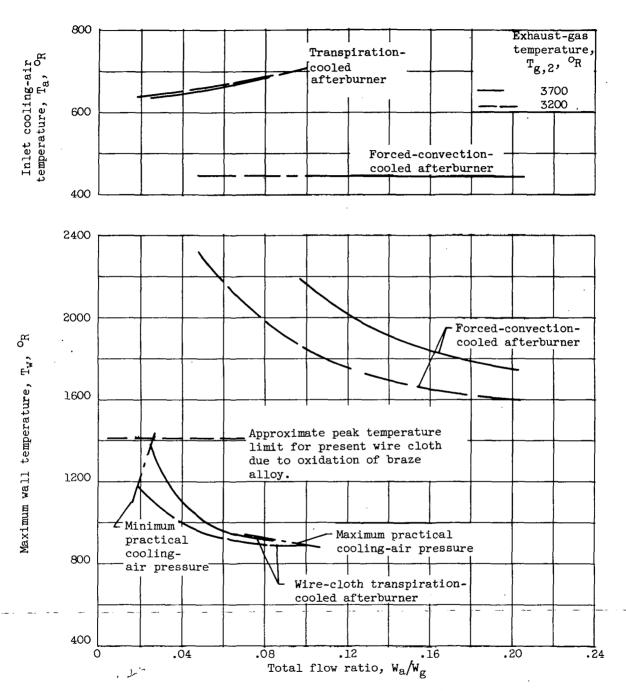


Figure 17. - Comparison of forced-convection and transpiration cooling applied to same afterburner. Uniform-permeability porous wall. Flight Mach number, 0.8; altitude 35,000 feet.

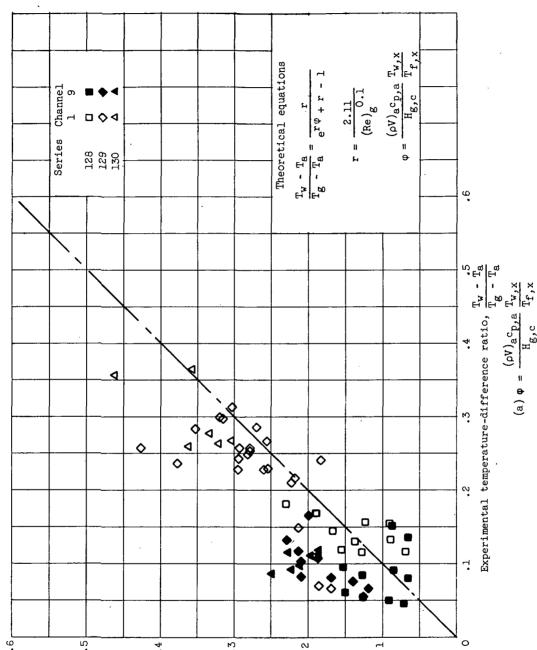
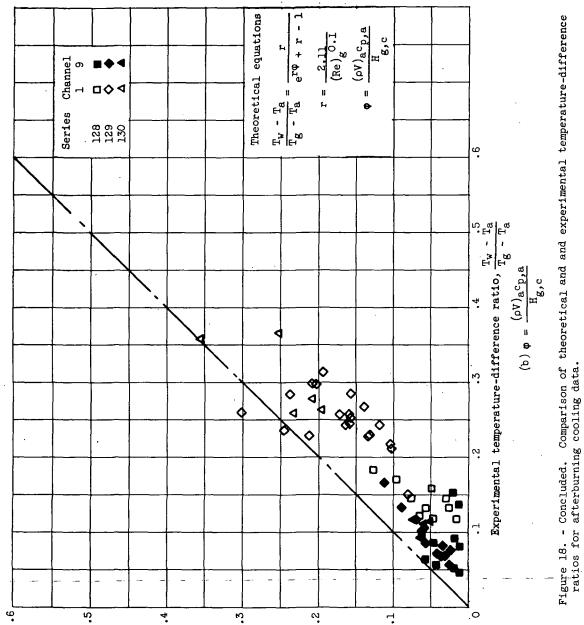


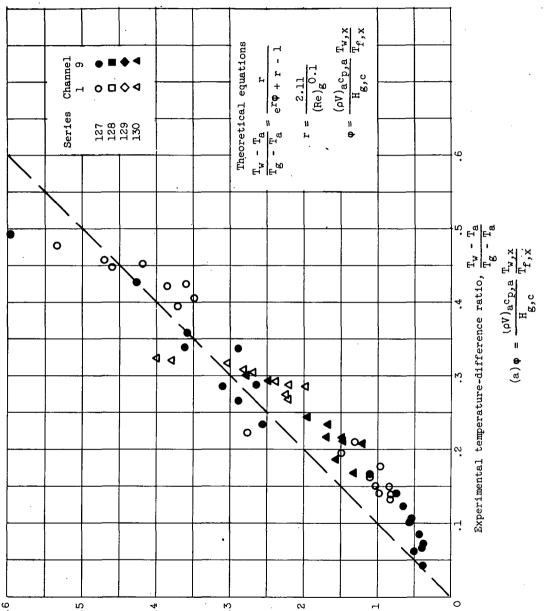
Figure 18. - Comparison of theoretical and experimental temperature-difference ratios for after-burning cooling data.

. Theoretical temperature-difference ratio,  $\frac{T_{\rm a}}{2T} - \frac{T_{\rm a}}{3T}$ 

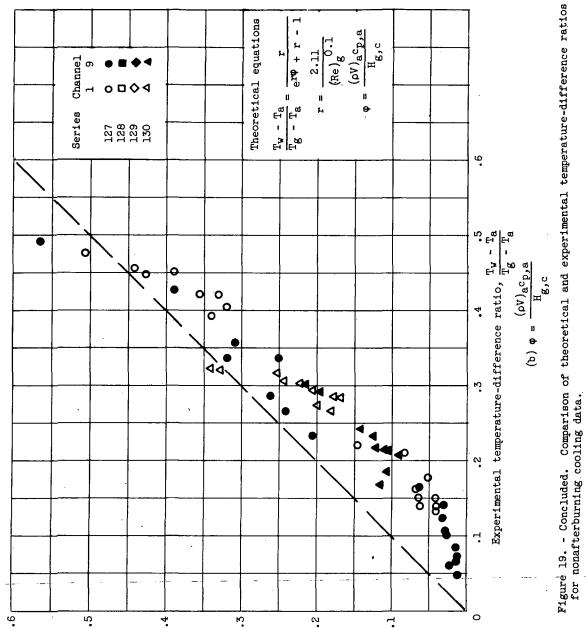


Theoretical temperature-difference ratio,  $\frac{T}{8} - \frac{T}{8}$ 

Figure 19. . Comparison of theoretical and experimental temperature-difference ratios for non-afterburning cooling data.



Theoretical temperature-difference ratio,  $\frac{T_a}{g^T} - \frac{T_B}{g}$ 



Theoretical temperature-difference ratio,  $\frac{T}{8} - \frac{T}{8}$ .

## CONFIDENTIAL

CLASSIFICATION CHANGED

By authority of MACA Reclassification
Wobice \$127 Date 6/5/58 100